从电子量子化到光子量子化的实验和应用

南京大学

陈坤基

2008年11月20日

提 要

- 引言：研究背景
- 量子点的构筑原理与技术
- 单电子效应及器件应用
- 光子量子点---光子量子化
- 展望

引言—研究背景

量子调控
- 量子计算　　量子位　　Qbit
- 量子通讯　　单光子　　Single Photon

基本物理原理
- 电子量子化
- 光子量子化

代表性的器件应用
- 单电子晶体管
- 单光子器件

原子中的电子行为

- 原子中电子的不连续性—电荷量子化

- 原子中电子轨道--能量量子化

人工微结构 -- 量子点、库仑岛 --人造原子

近年来，半导体超微细加工技术的高度发展已经能够制备出大小仅几个纳米的金属微粒或仅包含有几十个电子的半导体微粒。而在这些结构中的电子呈现出既不同单个原子中的电子也不同于宏观系统中的电子的异常现象。

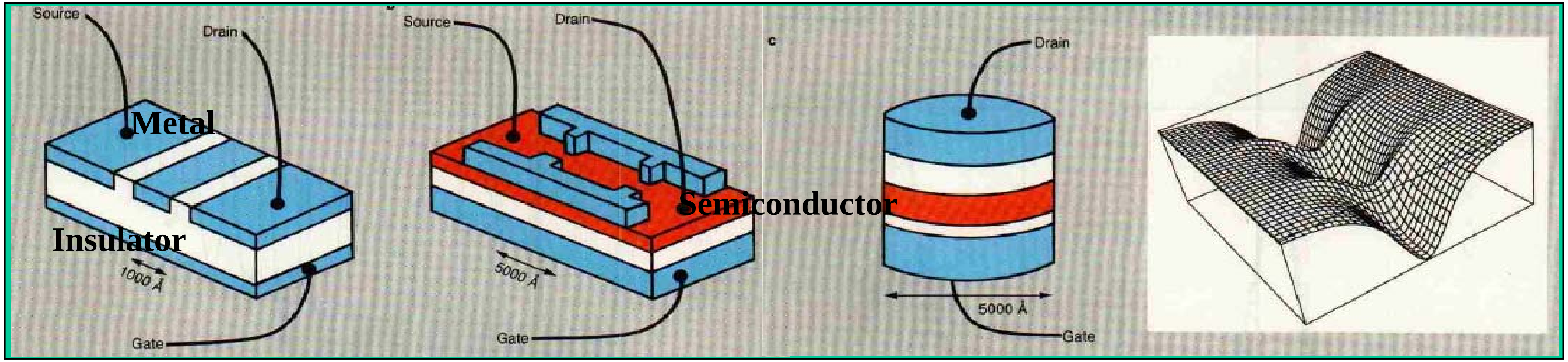

库仑岛　　单电子晶体管　　量子点　　电子的电势“阱”

这些人工设计的微结构被称作为量子点或库仑岛； 如果配以由隧道相联接的金属电极也被称为单电子晶体管。

人造原子中的电子特性？

- 自然原子中的电子数是不连续的（电荷量子化）
- 相应的电子能级也是不连续的（能量量子化）

那么人造原子中的电子是否也具有像自然原子中那样的电荷和能量量子化的特征？

电荷量子化：Charge Quantization

人们利用光电子谱测量了当原子中增加或移去电子时所需要的能量，例如我们熟悉的，从原子中移去一个电子所需要的最小光子能量称为电子的离化能；而当原子中增加一个电子而发射出的最大光子能量为电子的亲和势。

在研究人造原子时，我们也同样可利用测量在这种结构中增加或移去电子时所需要的能量来研究电荷量子化。

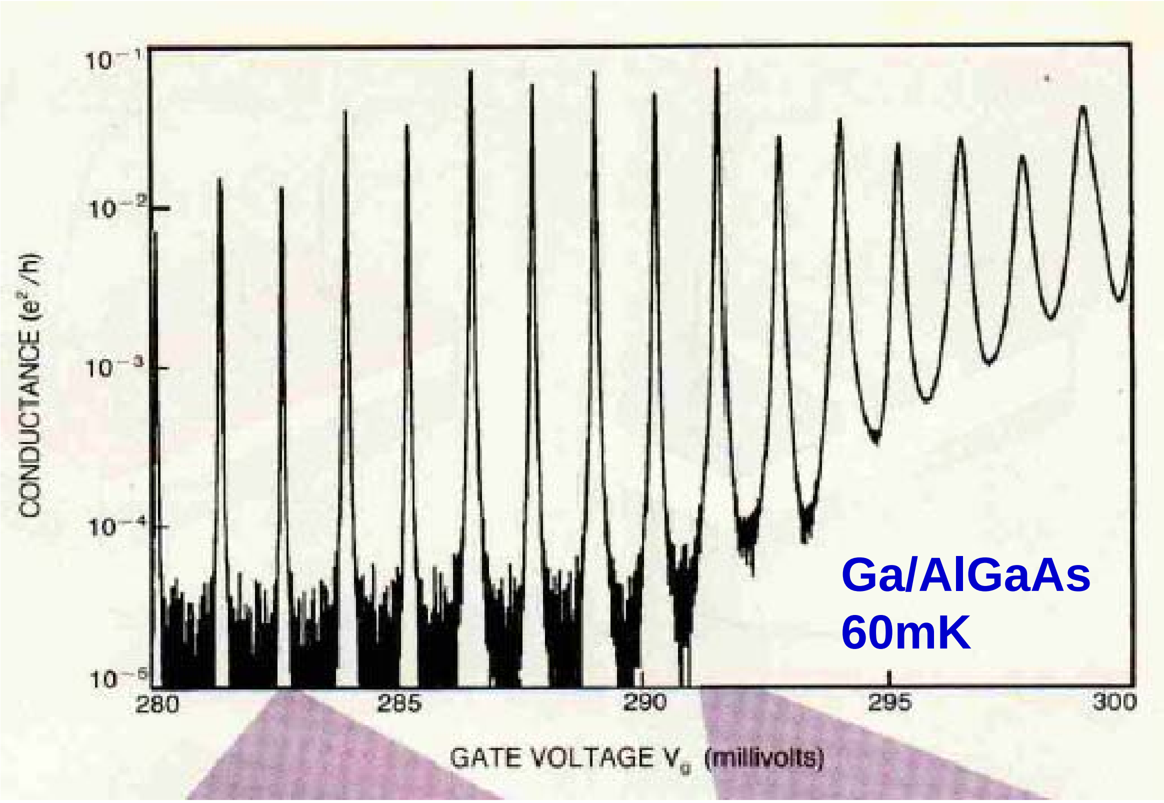

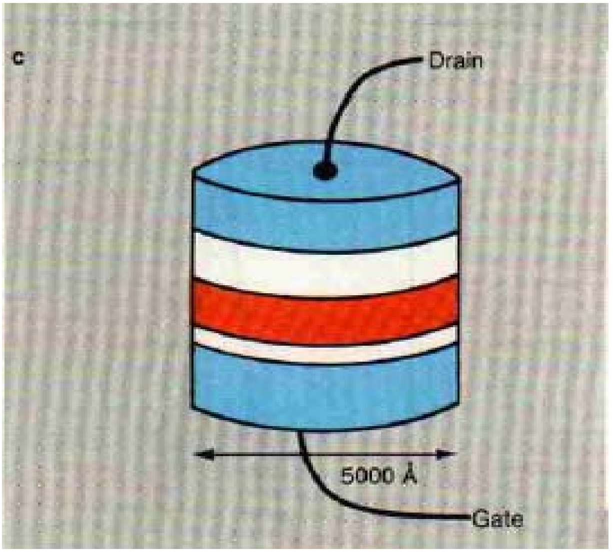

如图所示的是一个可控势垒结构的源漏电导与栅压Vg的函数关系，图中清楚地表明隧穿电导呈现出一系列明显的共振峰，且每个峰间距（ΔVg）几乎相等。通过计算纳米半导体与栅极之间的电容值表明ΔVg恰好是对该结构增加一个电子所需的能量。

如果把一个量子点当作一个电容为C的中性孤立系统，当要对系统充以电量为Q的电荷时，所需的能量为$Q^2/2C$。

因为电子是带电的最基本粒子，人们不可能增加或移去少于一个电子的电荷e，因此产生电流所需克服的库仑能即是$e^2/2C$。这个高度的势垒常被称为库仑阻塞能。

从抽象的意义上来讲，这种电子隧穿状态的不连续是人造原子中电子数不连续的结果，即电荷的量子化。

因此，如果测量的温度足够低，$KT<e^2/2C$，那么在人造原子结构中就能够观测到由电荷量子化产生的单电子（或空穴）的隧穿现象。

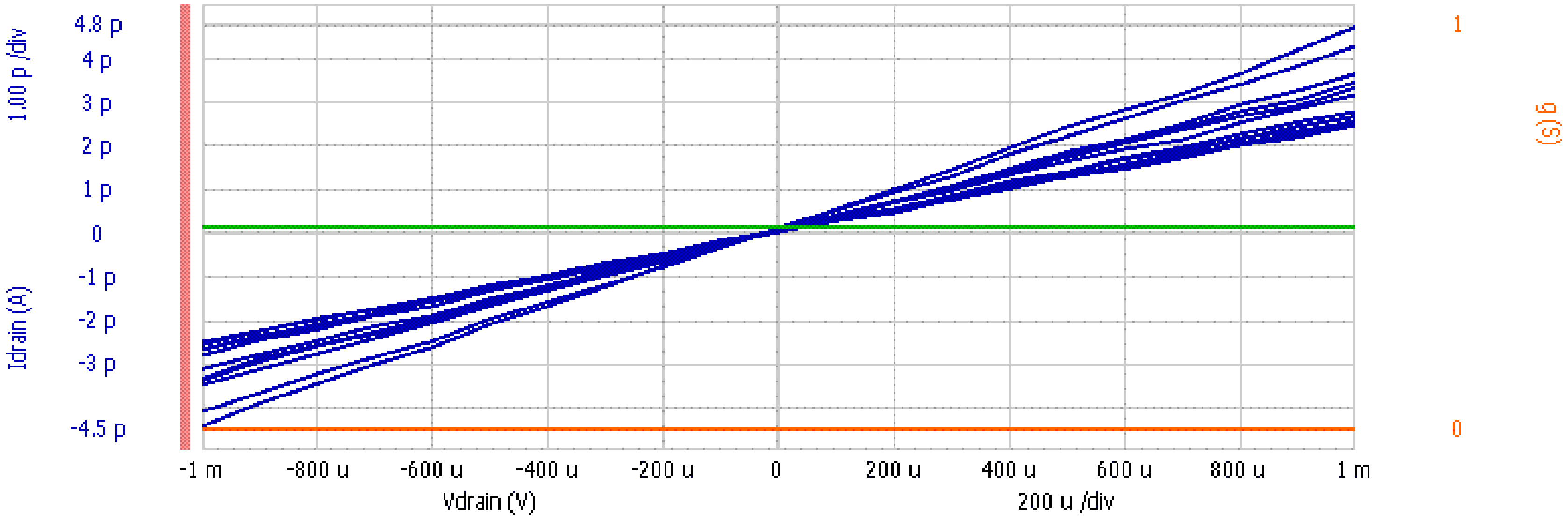

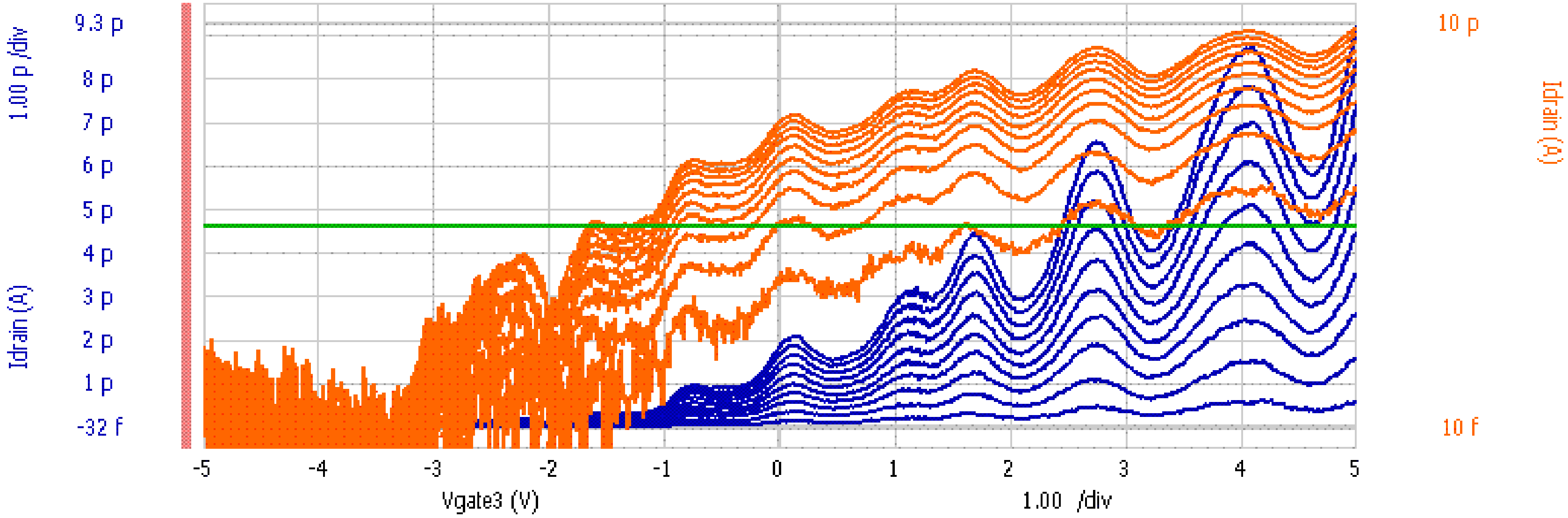

04-2@25K

NLSSMS

Nanjing University

能量量子化　Energy Quantization

当人造原子的尺寸小到德布罗意波长（de Broglie wave λ-50 nm）可比拟时，人造原子中的电子能级由于量子尺寸效应而产生不连续性。如果我们假设人造原子像一个边长为 a 的“盒子”，那么由量子力学计算得：最低能级之间得能量差为 $\hbar^2/ma^2$ 的数量级。

我们同样可以借助于测量在固定栅偏压 V_g 条件下隧道电流与源漏电压 V_{ds} 之间关系来检验这种能量不连续性。

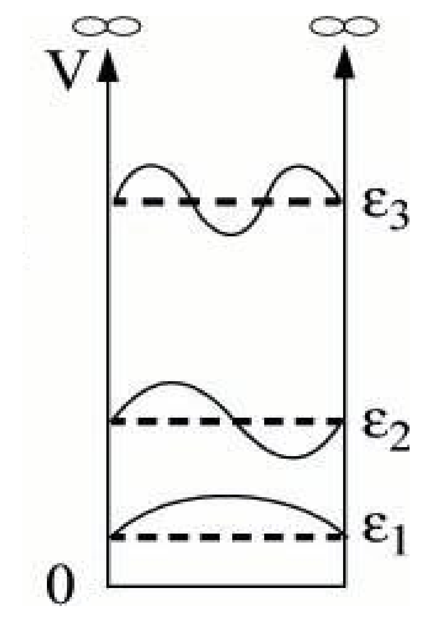

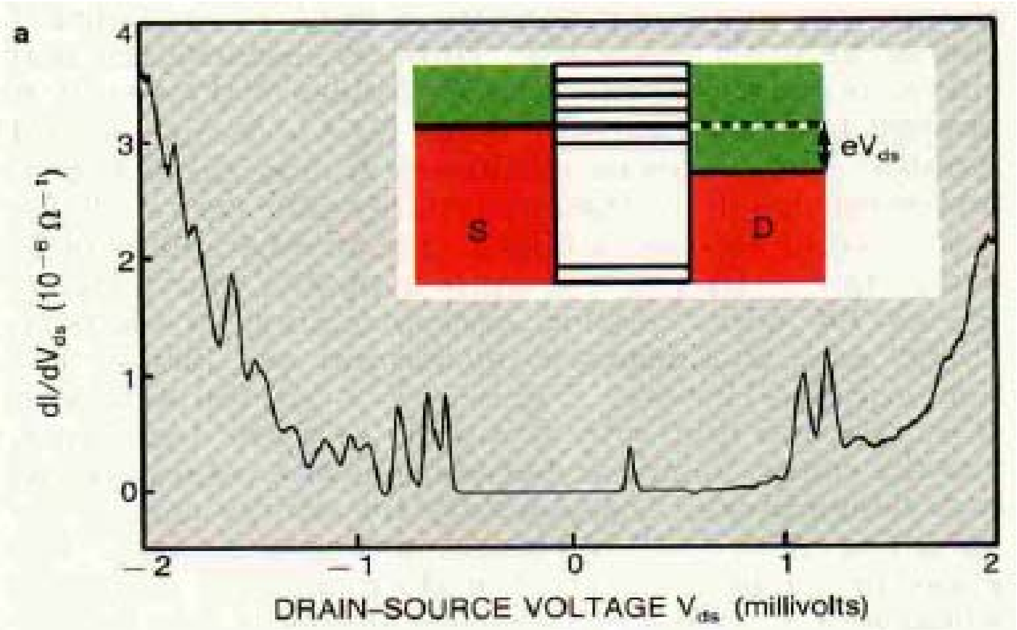

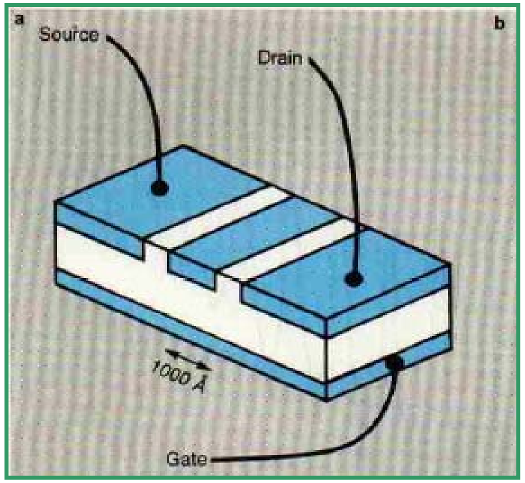

可控势垒人造原子的dI/dV_{ds}与V_{ds}的关系。

参看图中的能级示意图，随着V_{ds}的增加，源区的费米能级上升超过漏区的费米能级，并且当刚超过人造原子中的第一量子能级的能量时，电流便开始流动。当V_{ds}进一步增加，源区的费米能级将进一步上升，并逐次超过人造原子的高量子能级，随之有更多的能级成为电子通道，结果在流过的电流中产生与量子能级相对应的电流或电导峰。

- 采用现代纳米技术已能制备各种不同材料的量子点结构.

- 量子点结构呈现出明显的电荷量子化和能量量子化特性. 这是量子点应用于纳米量子电子器件和光电子器件的物理基础。

提 要

- 引言：研究背景
- 量子点的构筑原理与技术
- 单电子效应及器件应用
- 光子量子点---光子量子化
- 展望

Fabrication of Semiconductor quantum structures, Two distinct approaches

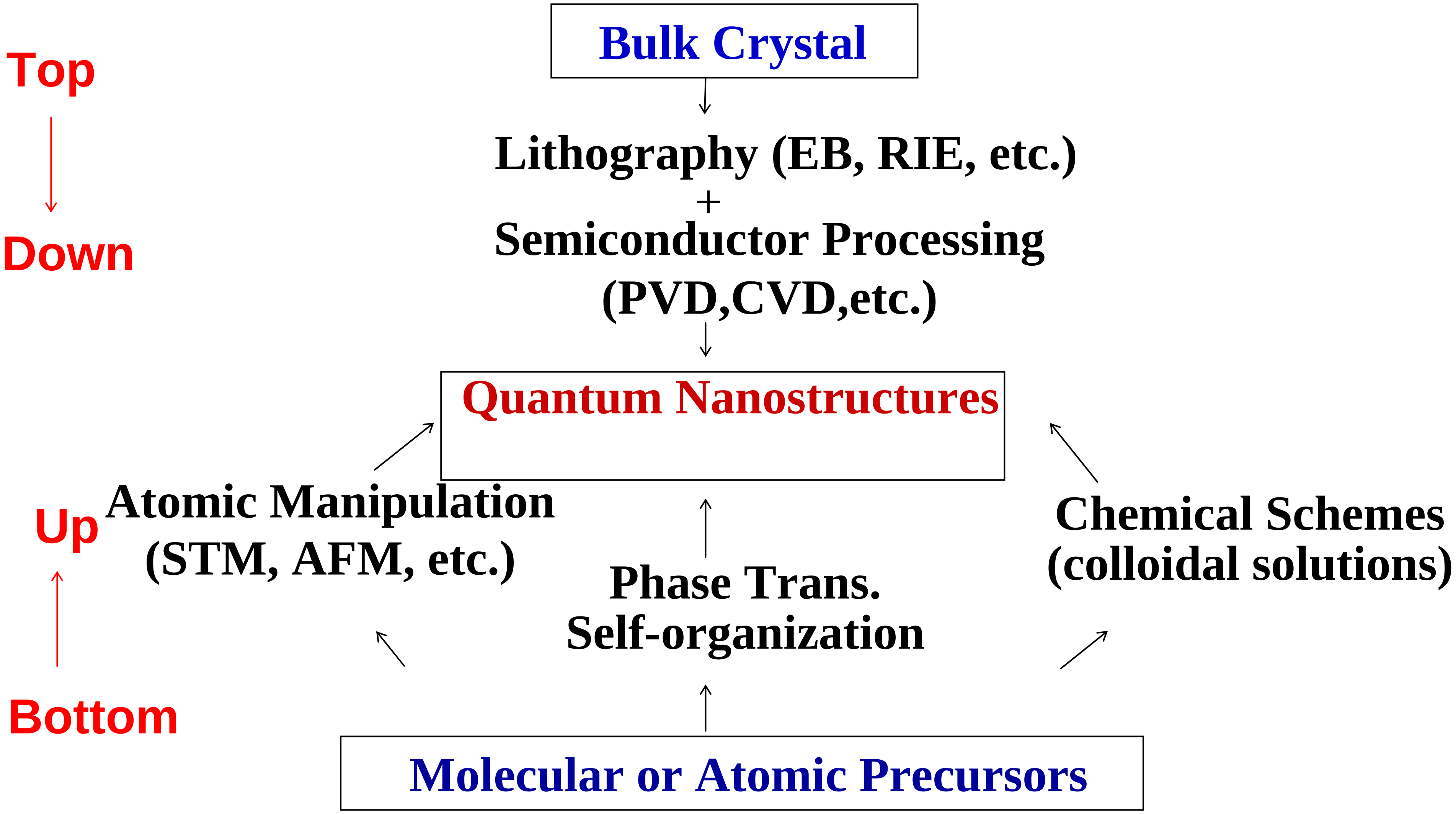

Top

Down

Bulk Crystal

Lithography (EB, RIE, etc.)
+
Semiconductor Processing
(PVD,CVD,etc.)

Quantum Nanostructures

Atomic Manipulation
(STM, AFM, etc.)

Phase Trans.
Self-organization

Chemical Schemes
(colloidal solutions)

Up

Bottom

Molecular or Atomic Precursors

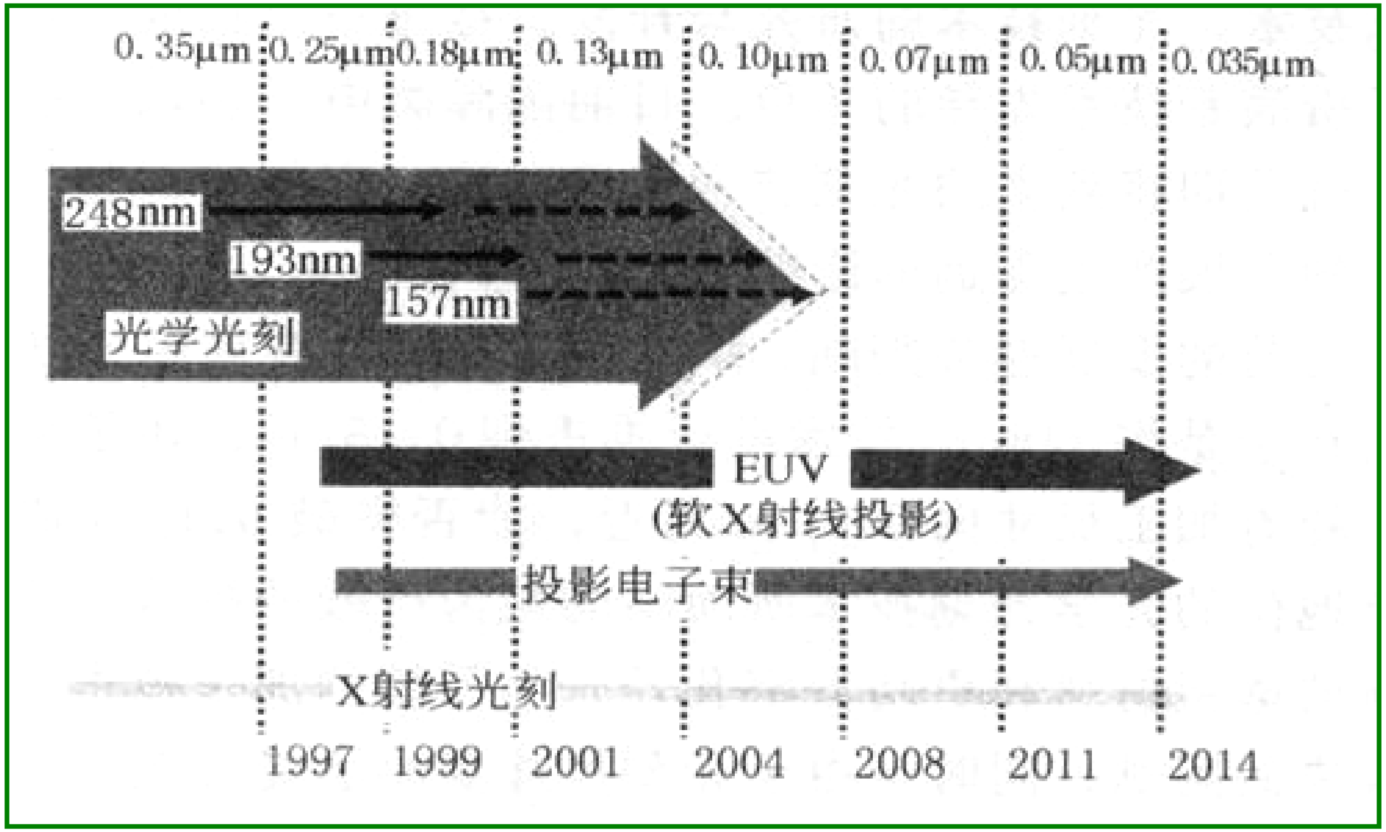

各种光刻技术可达到的分辨率比较示意图

Nanolithograpy by Using PS Ball Mask

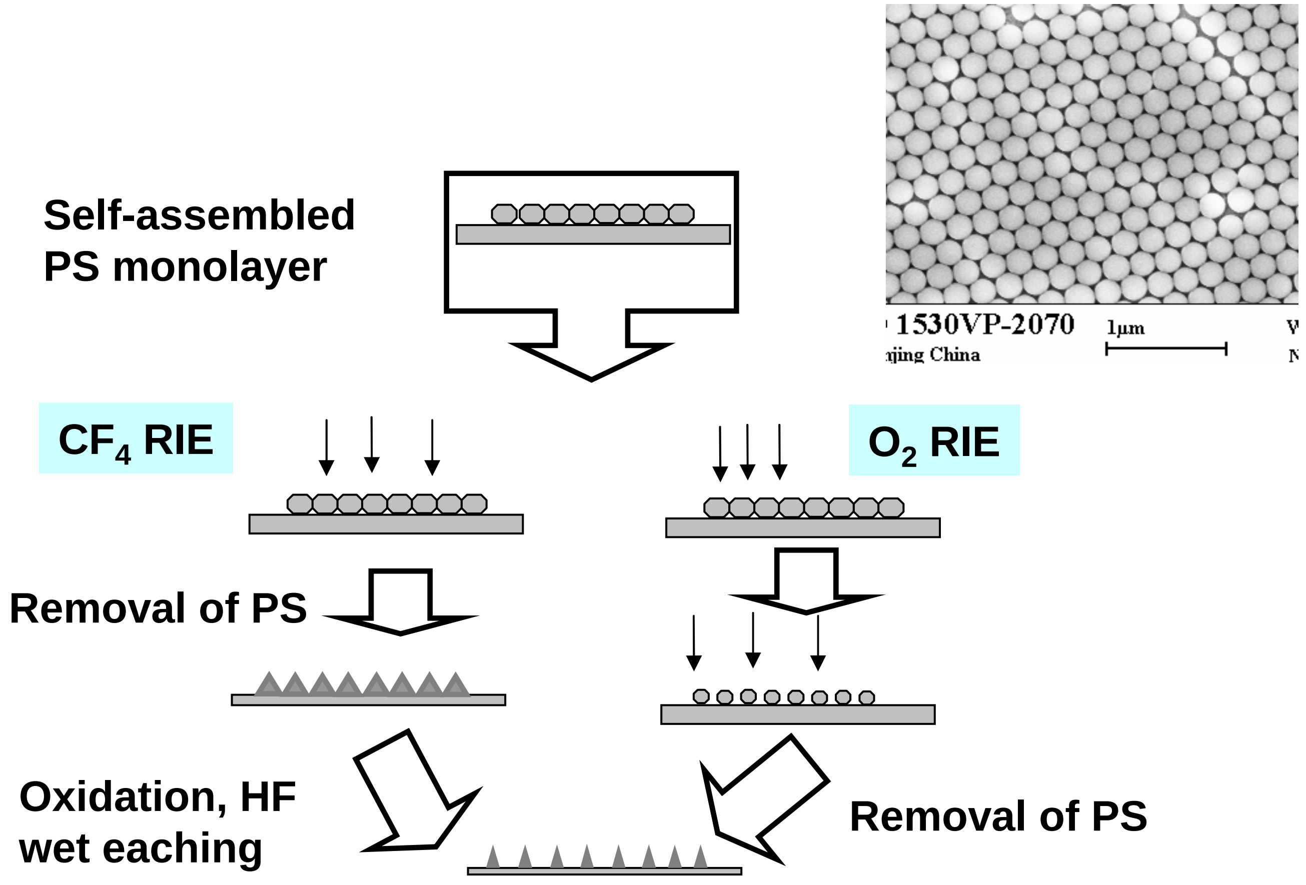

Self-assembled
PS monolayer

CF_4 RIE

O_2 RIE

Removal of PS

Oxidation, HF
wet eaching

Removal of PS

Ordered nc-Si QD Array by Nanolithograpy

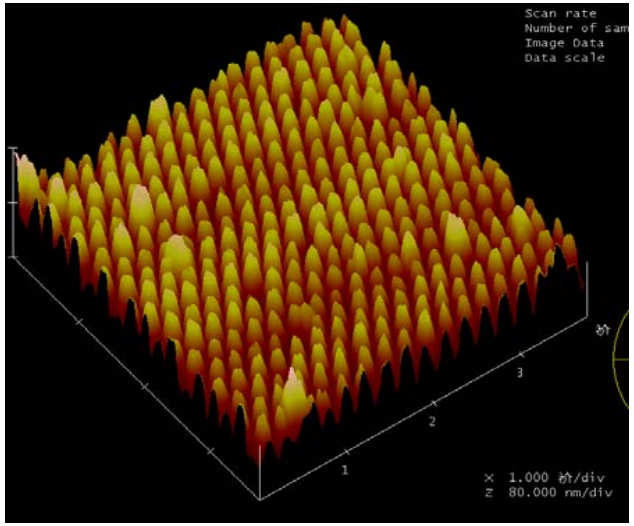

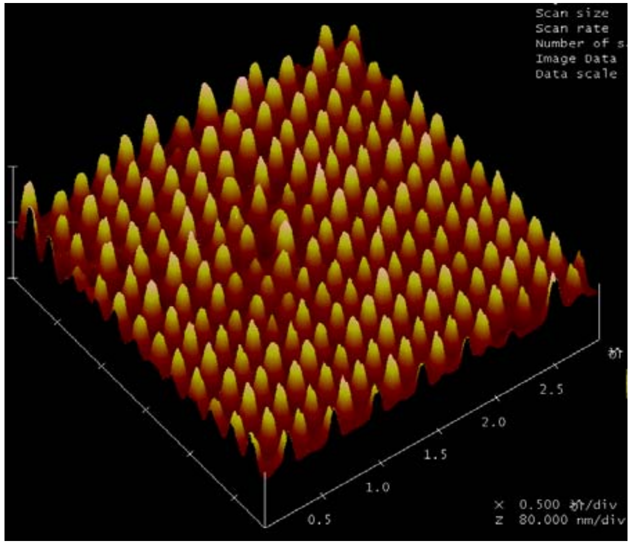

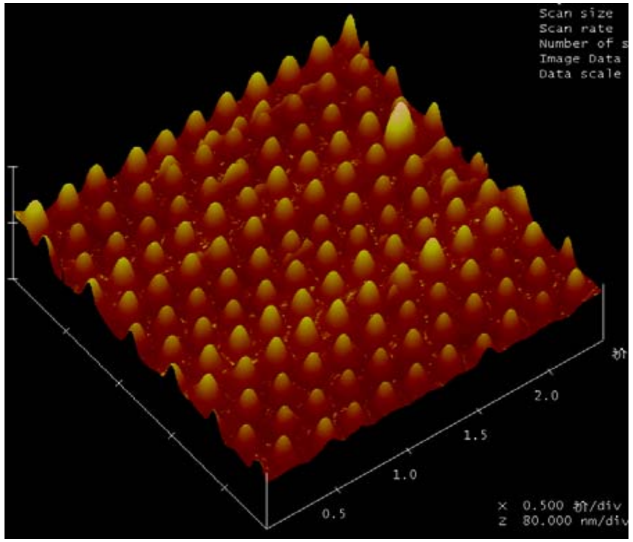

Z 80 nm/div

AFM Image

Chemical Synthesis of Monodisperse Nanoparticles

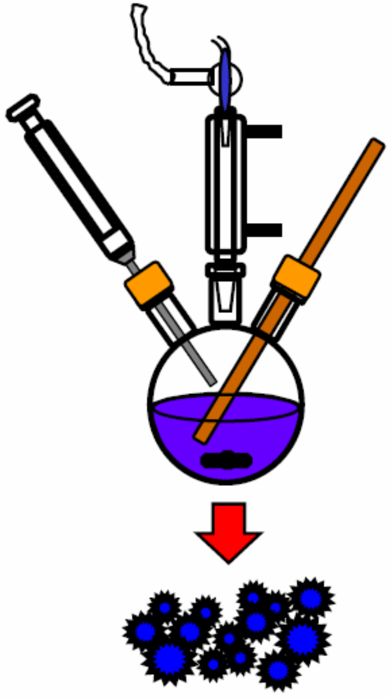

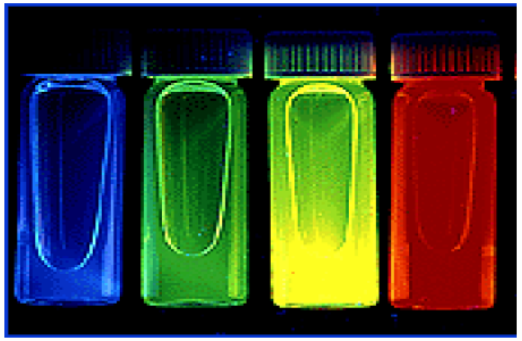

5 nm σ <5% CdSe Nanocrystals

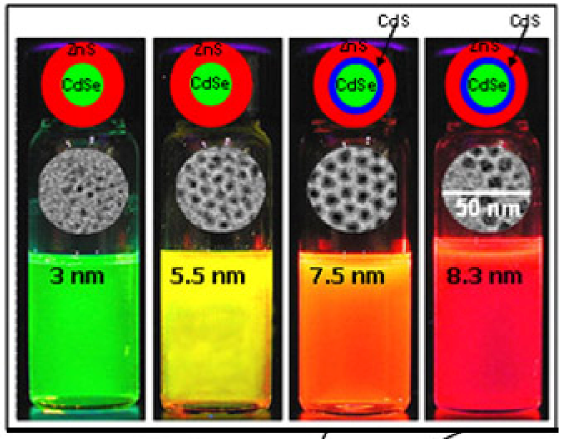

Technique Challenge

However, the open question is that can nano-crystal semiconductor leave laboratories and be adopted by a real fabrication line?

The most important need is to find a preparing technique that can combine

- precise control of nanocrystal sizes and positions
- excellent surface passivation
- compatible with the current Si ULSI technology

For realizing the above goal our group first proposed:

to use the principle on interface constrained growth of nc-Si from ultra-thin a-Si layer within the sandwich or multilayer structures to control the crystallite size and the position

Ordered Controllable Array of nc-si Dots

The Idea of Constrained Crystallization for Preparing nc-Si from a-Si

Vertical Constraint:

Multilayer ⟶ Control the thickness of a-Si sublayer

⟶ Longitudinal size of nc-Si

Lateral Constraint:

Phase shift grating ⟶ Interference laser beam

⟶ Local crystallization

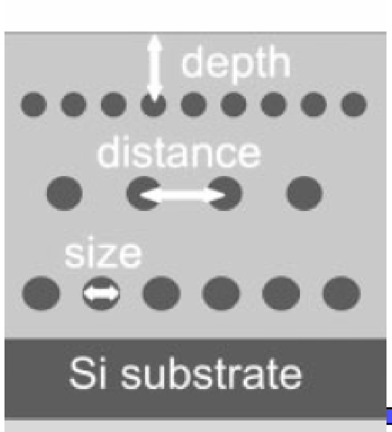

1D、2D and 3D ordered nc-Si array

MODEL OF INTERFACE CONSTRAINED GROWTH

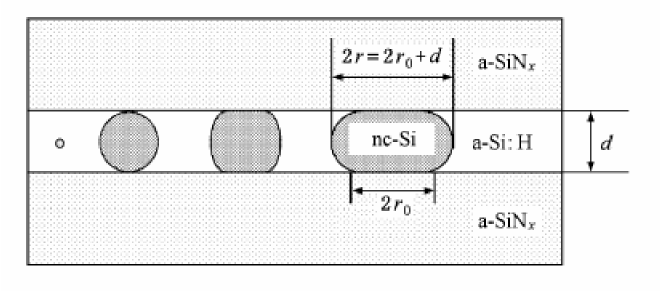

(a)

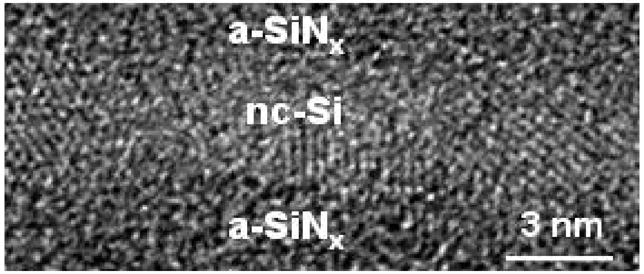

(c)

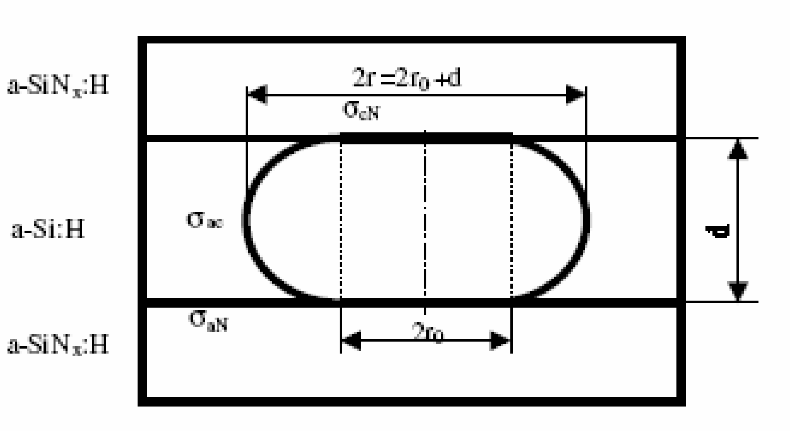

(b)

(a) The scheme for the processes of nucleation and growth of nc-Si.
(b) The cross-section shape of a typical nc-Si grain.
(c) A cross-section TEM image of the nc-Si sublayer.

MODEL OF INTERFACE CONSTRAINED GROWTH

We study quantitatively the effects of the interface and shape of nc-Si on the crystal growth in relation to the Gibbs free energy G.

For a spherical crystallite:

$$\Delta G_{sp} = -\frac{4}{3}\pi r^3(\Delta H_{ac} + \Delta H_s) + 4\pi r^2\sigma_{ac}$$

For a cylindrical crystallite:

$$\Delta G_{cy} = -\pi r^2 d\Delta H_{ac} + 2\pi r d\sigma_{ac} + 2\pi r^2\left(\sigma_{cN} - \sigma_{aN}\right)$$

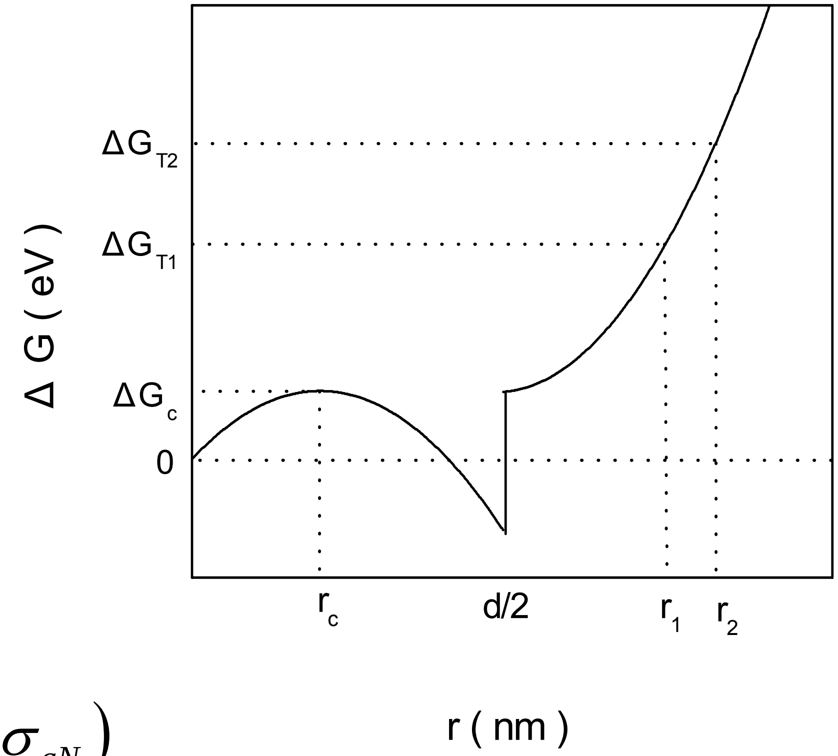

Schematic diagram of free energy change of nc-Si accompanying the crystallization process

MODEL OF INTERFACE CONSTRAINED GROWTH

$\Delta G(r)/\Delta r < 0$, the grains can grow continuously

$\Delta G(r)/\Delta r > 0$, the growth halt will occur

$\Delta G(r)/\Delta r = 0$, obtain the threshold thickness d_0

$$d_0 = 2\Delta\sigma / \Delta G_{ac}$$

~ 25 nm

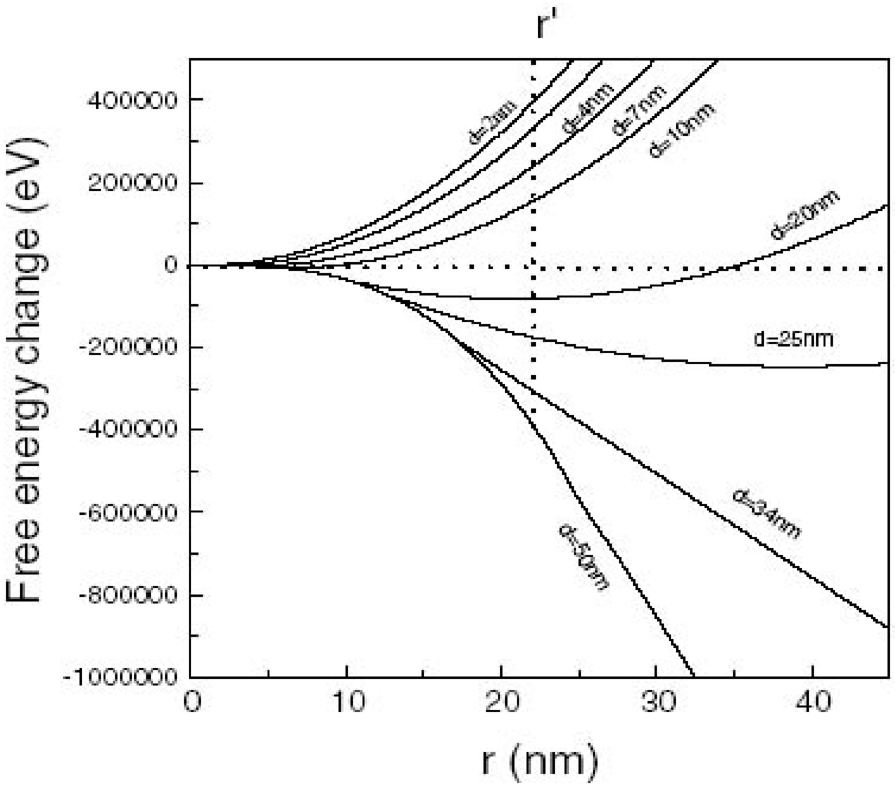

The free energy change dependence of the nc-Si grain radius at various thicknesses of a-Si sublayers.

Formation of nc-Si Superlattice by Constrained Growth

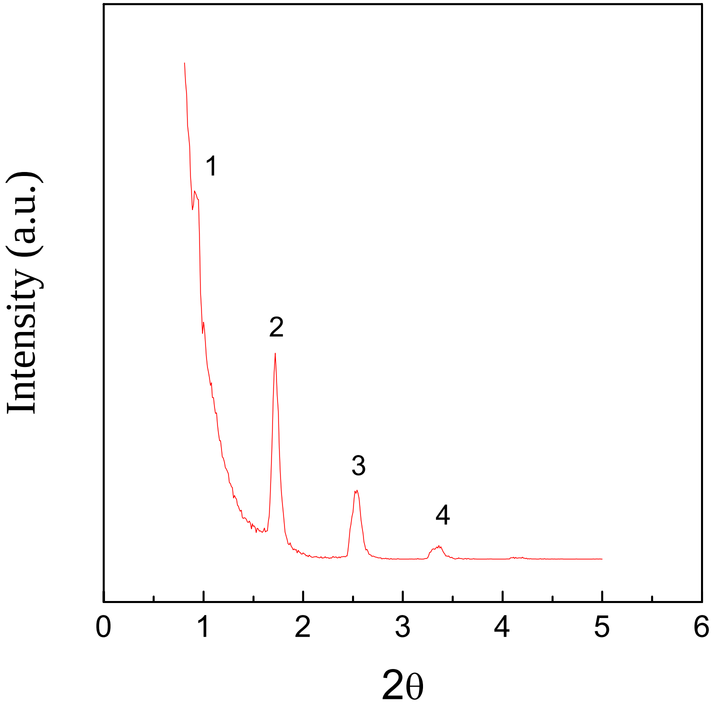

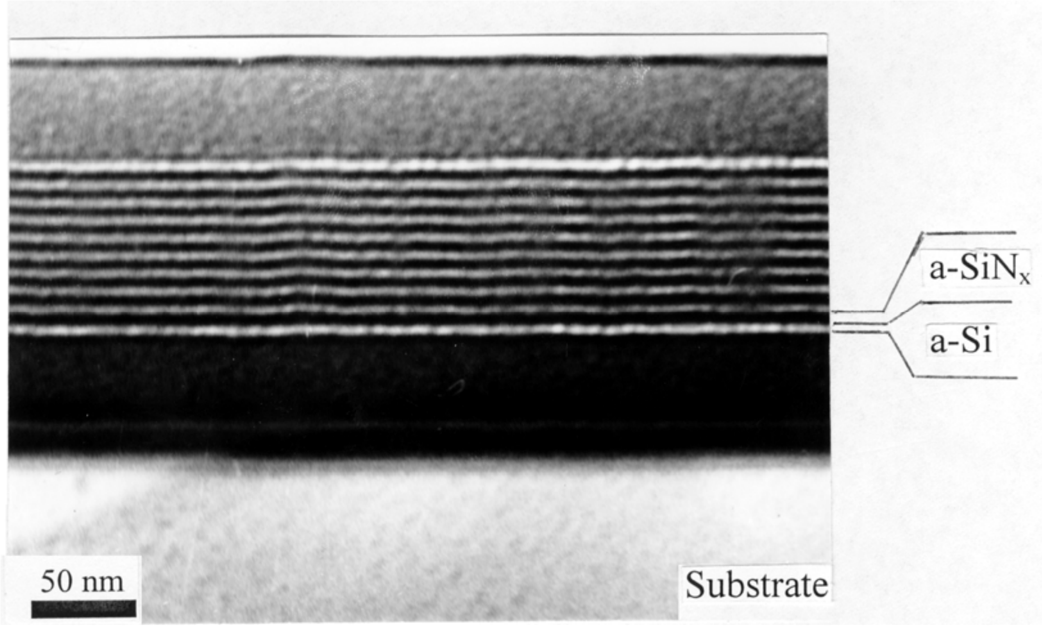

XRD and TEM micrographs of a-Si/a-SiN$_x$ multilayers and Si QDs embedded in SiN$_x$ matrix. The average size of Si QDs is about 4.0 nm.

Ordered Controllable Array of nc-si Dots

Formation of nc-Si Superlattice by Constrained Growth

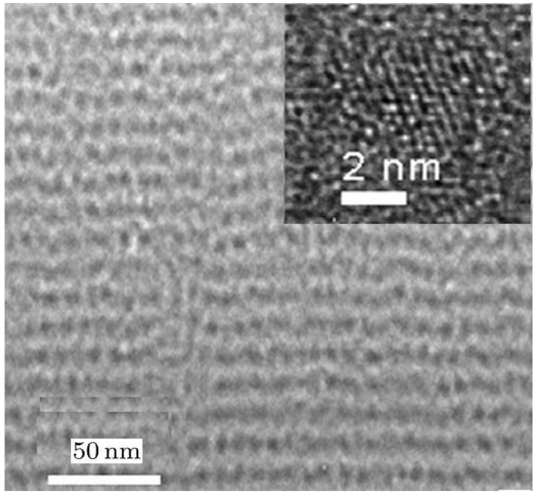

Si/SiO_2 Superlattice

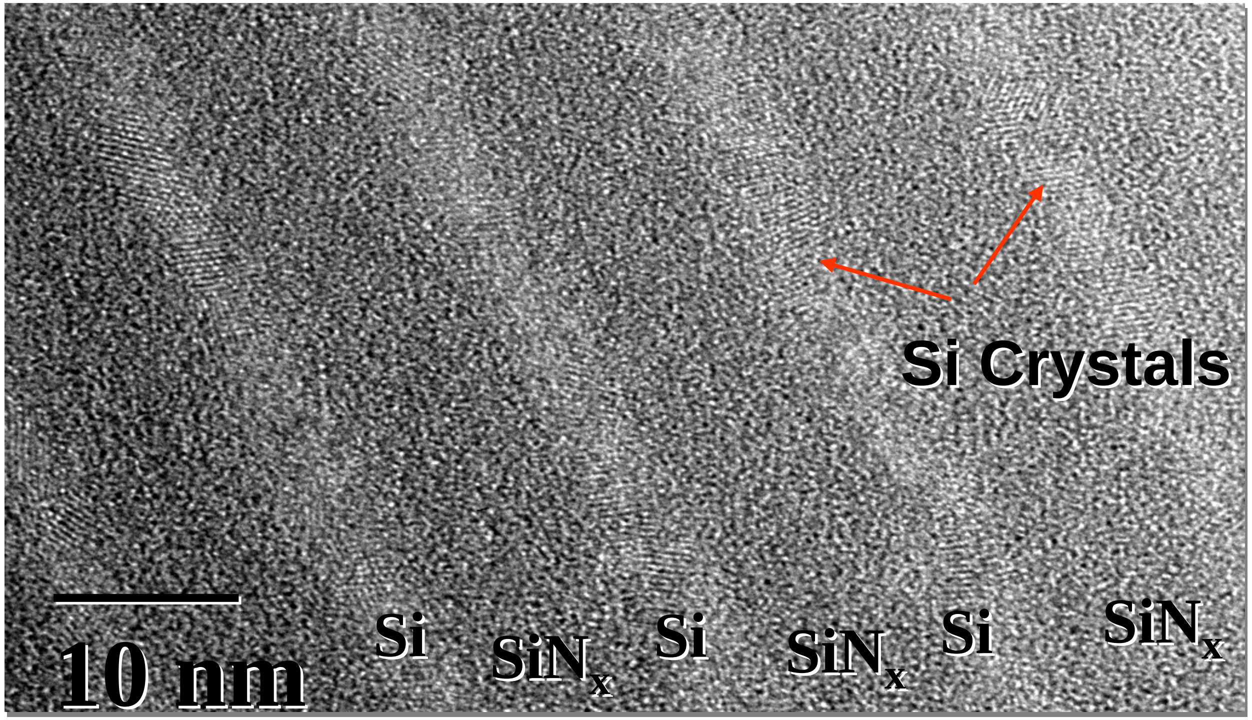

Cross-section HRTEM of nc-Si Superlattice

1D、2D and 3D ordered nc-Si structures

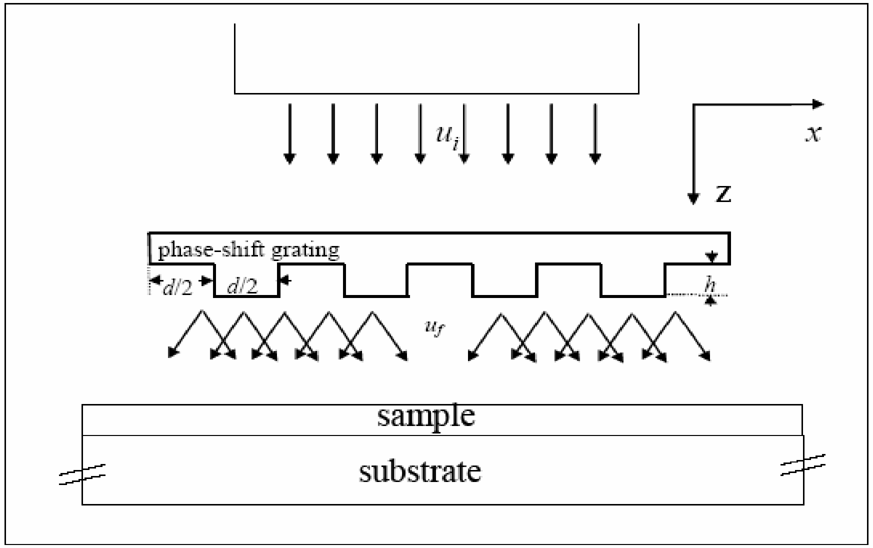

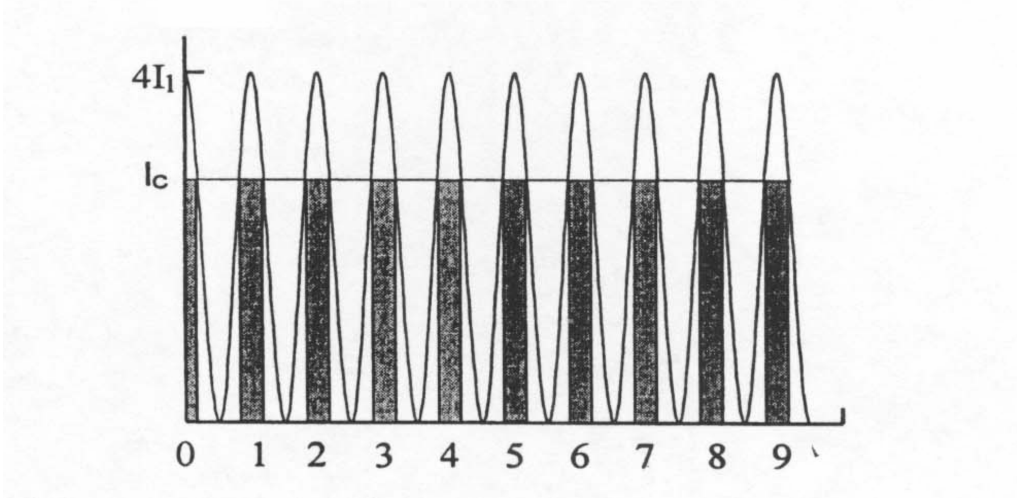

The sketch diagram for the laser interference method. KrF excimer laser beam passes at normal incident through the phase-shifting grating placed on the surface of the sample, then the separate Lorentz-like energy packages are formed due to the multi-beam interference. When the local laser intensity exceeds the crystallization threshold value, crystallization process occurs in the shadowed areas.

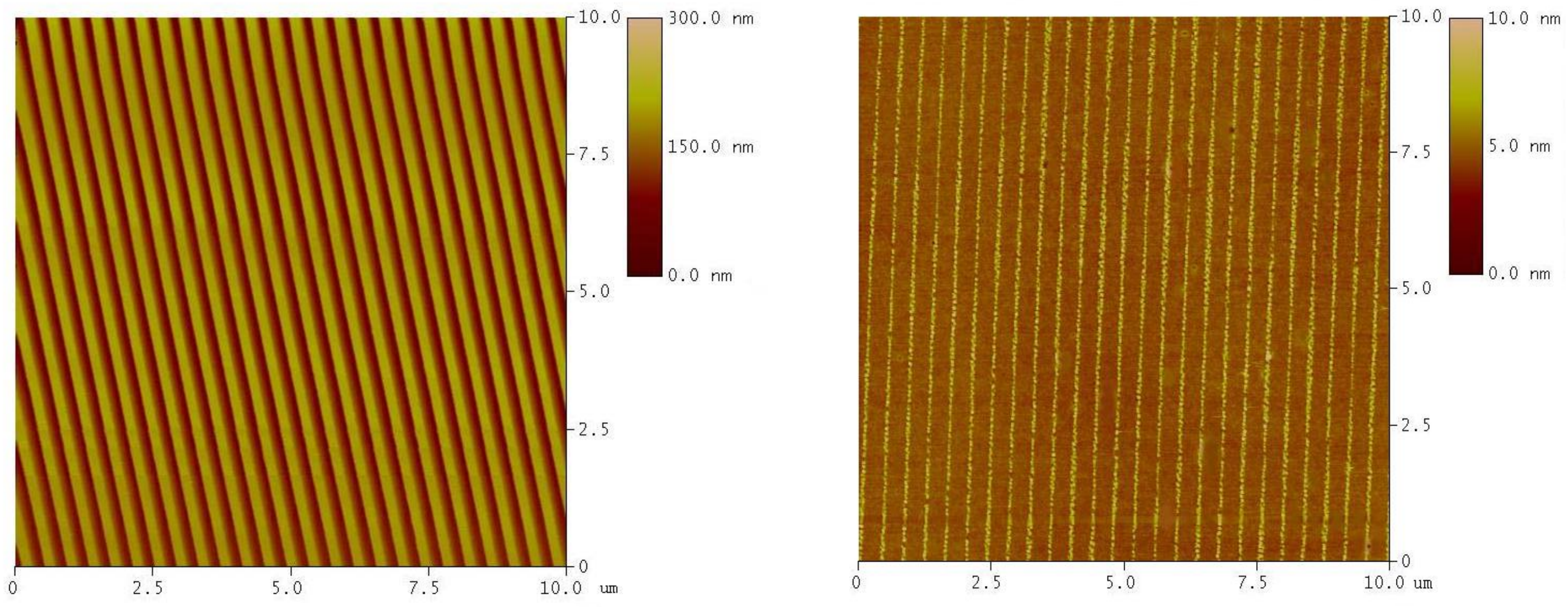

The surface morphology of 1D grating and an irradiated sample.

The bright stripes (crystallized regions)

width < 30 nm, periodicity ~ 400 nm;

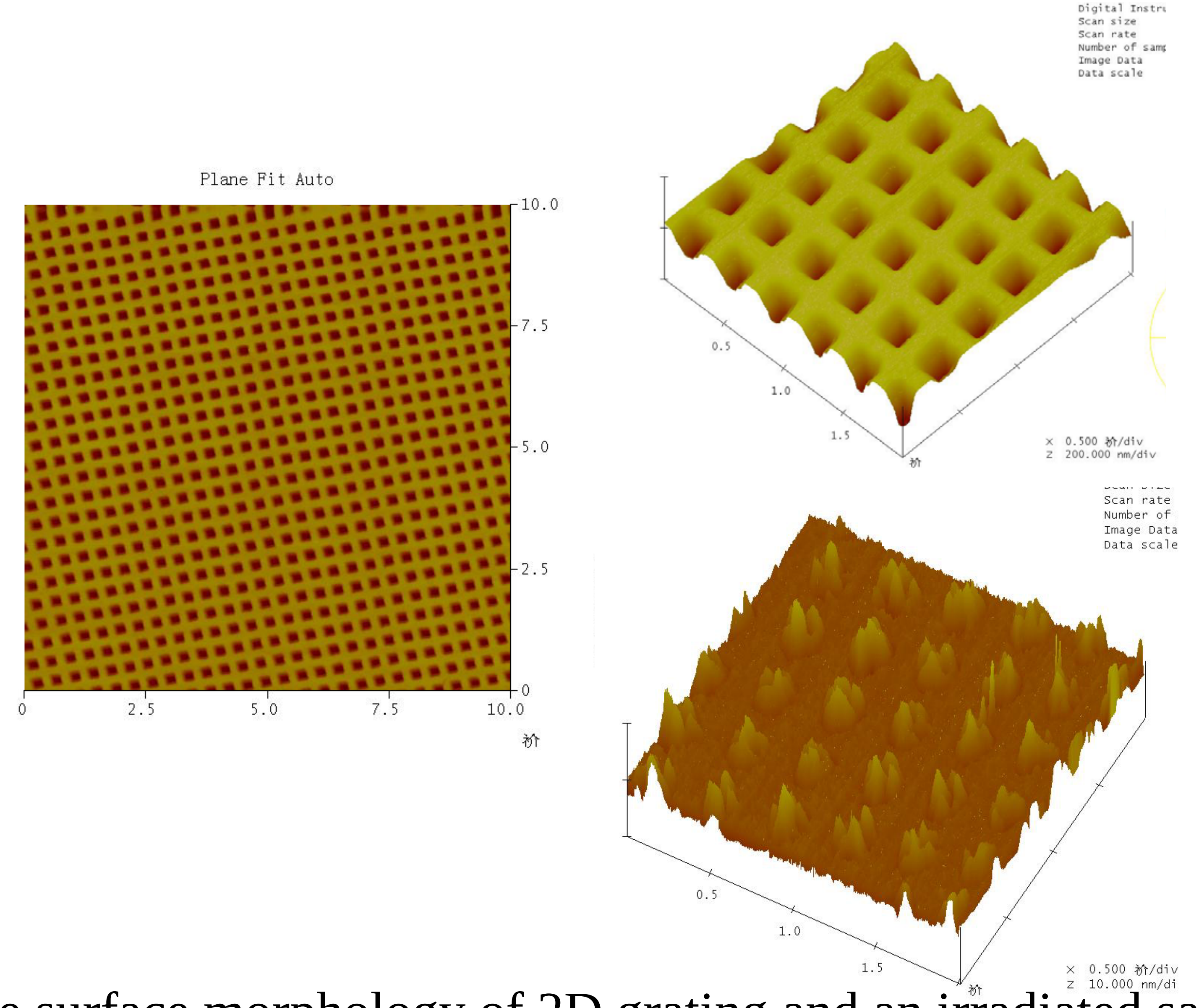

The surface morphology of 2D grating and an irradiated sample.

Adv.Mater. 2005,17, No.7, 795-803

REVIEW

ADVANCED MATERIALS

Silicon Nanocrystals: Size Matters**

By *Johannes Heitmann, Frank Müller,*
*Margit Zacharias,** and *Ulrich Gösele*

Max-Planck-Institut für Mikrostrukturphysik
Weinberg 2, D-06120 Halle (Germany)

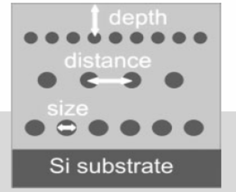

1. Introduction

The first experimental results more than a decade ago demonstrating room-temperature luminescence of silicon nanocrystals (Si-NCs) in silicon-implanted SiO_2[1] or in porous silicon[2,3] triggered a strong interest in the fabrication of Si-NCs and their properties. Besides fundamental physics questions concerning quantum-confinement effects in the indirect semiconductor silicon,[4–7] potential applications such as light emission from electrically excited Si-NCs,[8–13] energy transfer to Er^{3+} ions,[14–19] and non-volatile memory devices[20,21] also stimulated a broad interest in this material system. For clarifying

Electroluminescence (EL) measurements on all sorts of Si-NCs show efficiencies below 1×10 [8–13] This makes electri-

[12] M. Wang, X. Huang, J. Xu, W. Li, Z. Liu, K. Chen, *Appl. Phys. Lett.* **1998**, *72*, 722.

APPLIED PHYSICS LETTERS VOLUME 72, NUMBER 6 9 FEBRUARY 1998

Observation of the size-dependent blueshifted electroluminescence from nanocrystalline Si fabricated by KrF excimer laser annealing of hydrogenated amorphous silicon/amorphous-SiN_x:H superlattices

Mingxiang Wang, Xinfan Huang, Jun Xu, Wei Li, Zhiguo Liu, and Kunji Chen[a)]

3. Size-Controlled Silicon-Nanocrystal Synthesis

3.1. Amorphous Silicon/Insulator Superlattices

The use of Si/SiO_2 superlattices was first introduced by Lockwood and co-workers.[57,58] In this technique, molecular-beam epitaxy (MBE) combined with oxidization by UV/mass approximation. Later, similar systems could be realized by reactive magnetron sputtering or co-sputtering,[59–63] plasma-enhanced (PE)CVD or low-pressure (LP)CVD,[64–66] or reactive evaporation.[67] After the crystallization of the amor-

[65] Z. Ma, L. Wang, K. Chen, W. Li, L. Zhang, Y. Bao, X. Wang, J. Xu, X. Huang, D. Feng, *J. Non-Cryst. Solids* **2002**, *299*, 648.

for bulk silicon.[62,70] A combination of this controlled deposition method with a patterning of the resulting layered structure comparable to other microelectronic devices is possible.[71,72]

[71] L. Y. Zhu, X. F. Huang, W. B. Fan, X. W. Wang, W. Li, L. Wang, K. J. Chen, *Superlattices Microstruct.* **2002**, *31*, 285.

[76] L. Wang, Z. Ma, X. Huang, Z. Li, J. Li, Y. Bao, J. Xu, W. Li, K. Chen, *Solid State Commun.* **2001**, *117*, 239.

[77] H. Huang, L. Wang, J. Li, W. Li, M. Jiang, J. Xu, K. Chen, *J. Non-Cryst. Solids* **2000**, *266–269*, 1015.

silicon evaporation and periodic electron cyclotron resonance plasma nitridation,[74] by excimer pulsed-laser deposition,[12,75] and by LPCVD.[76,77] $Si/Si_xO_yN_z$ superlattices were produced

These controlled deposition methods led to a number of diode-like structures for electrically pumped devices.[12,81–83] Also, for the EL measurements, different signal wavelengths between 500 and 900 nm were reported; these were mainly attributed to hot-impact ionization of excitons confined in the Si-NCs. This explanation could not be proved in detail and is still under discussion. The reported quantum efficiencies of electroluminescence do not exceed 1×10^{-3}.

提 要

- 引言：研究背景
- 量子点的构筑原理与技术
- 单电子效应及器件应用
- 光子量子点---光子量子化
- 展望

Ω

The collective single-electron Coulomb blockade effects in the single layer nc-Si array

➢ Structure

The SiO_2/nc-Si QDs array/SiO_2/n^+-Si structure is fabricated in a plasma enhanced chemical vapor deposition (PECVD) system.

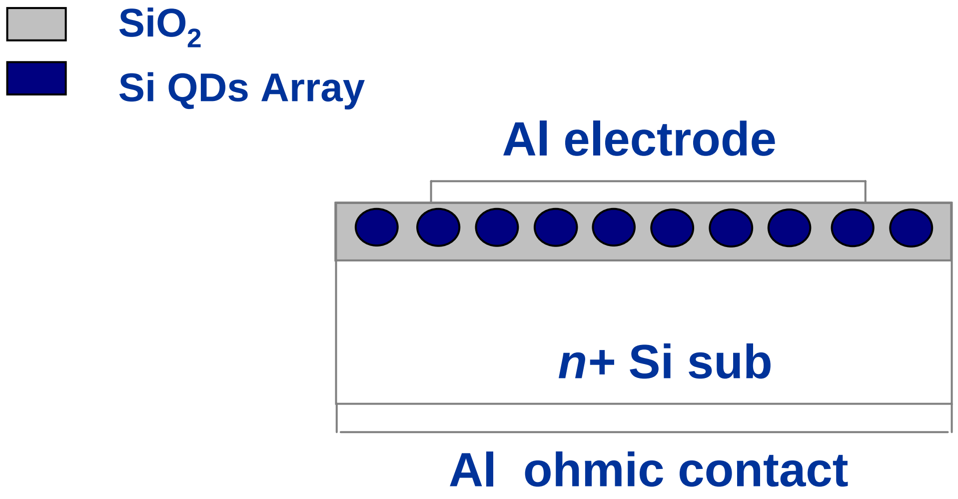

▨ SiO_2

■ Si QDs Array

Al electrode

n+ Si sub

Al ohmic contact

Schematic diagram of the structure

Electrode area:
0.8×10^{-3} cm^2

Substrate:
n^+- Si (100)
p - Si (100)

➢ AFM image

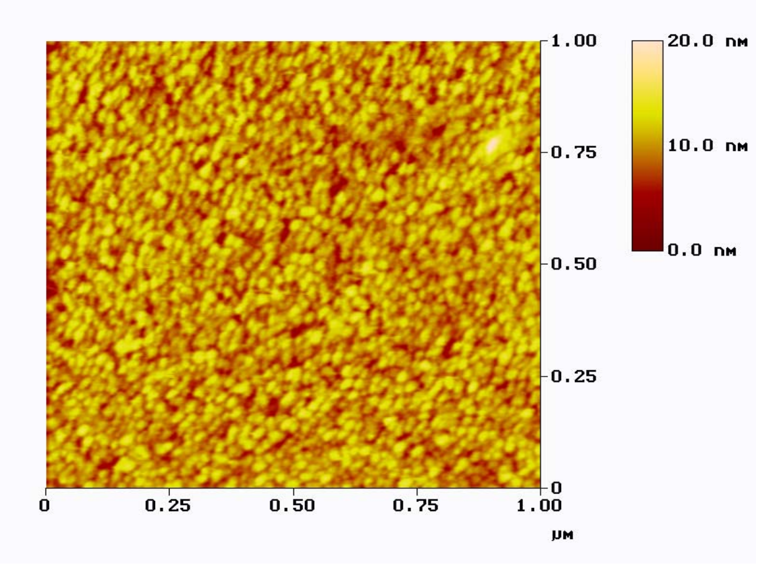

AFM image of nc-Si after removing the gate oxide.

➢ X-TEM

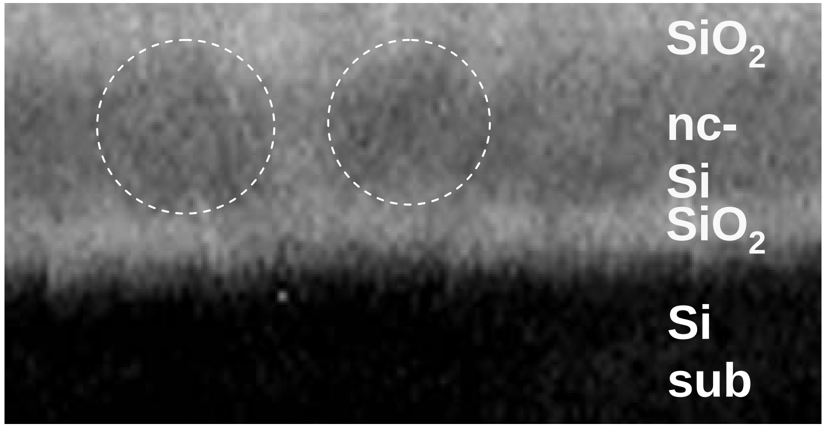

Cross section TEM photograph of sample structure

The density and the mean diameter are 2×10^{11} cm^{-2} and 6 nm, respectively.

➢ I-V characteristics

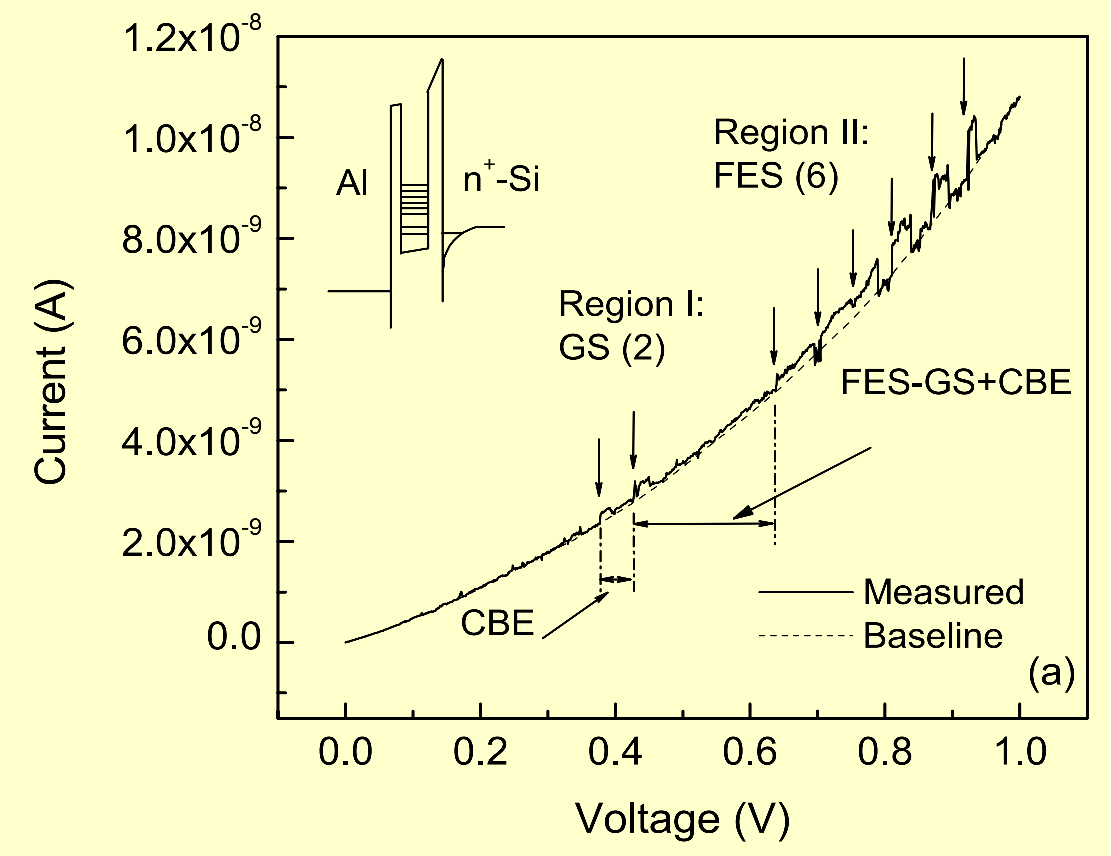

* **Unique platform-like peaks**

* **Distribution**

- **Spacing between peaks**
- **Spacing between regions**

GS: **Ground State**

FES: **First Excited State**

CBE: **Coulomb Blockade Energy**

A typical I-V curve with "sharp-edged platform-like" peaks, which are divided into two regions according to their positions in voltage. The schematic band diagram is shown in the up-left inset.

➢ I-V characteristics

CBE and QCE

Confinement Levels	GS (2)		FES (6)					
Peak No.	1	2	1	2	3	4	5	6
Peak Position (V)	0.38	0.43	0.64	0.70	0.76	0.81	0.87	0.93
Between Peaks(V)	---	0.05	---	0.06	0.06	0.05	0.06	0.06
Between Region(V)	---	---	0.14	---	---	---	---	---

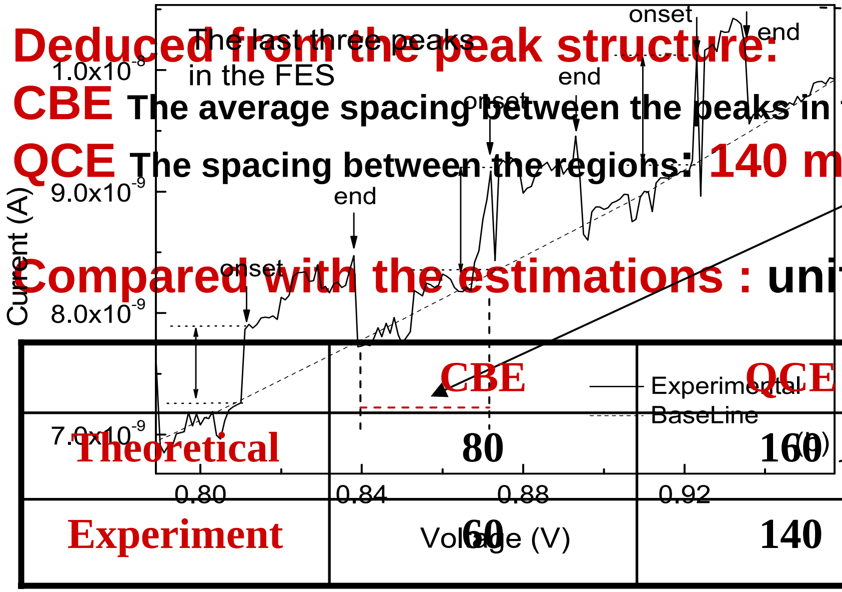

Deduced from the peak structure:

CBE The average spacing between the peaks in the same region：**60 meV**,

QCE The spacing between the regions: **140 meV**

Compared with the estimations : unit meV

	CBE	QCE
Theoretical	80	160
Experiment	60	140

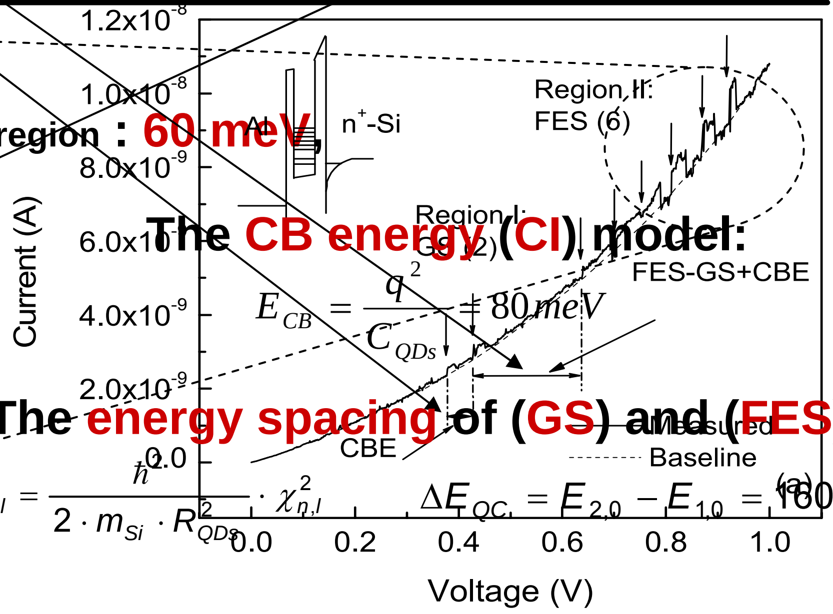

The CB energy (CI) model:

$$E_{CB} = \frac{q^2}{C_{QDs}} = 80\,meV$$

The energy spacing of (GS) and (FES):

$$E_{n,l} = \frac{\hbar^2}{2 \cdot m_{Si} \cdot R_{QDs}^2} \cdot \chi_{n,l}^2 \qquad \Delta E_{QC} = E_{2,0} - E_{1,0} = 160\,meV$$

➢ C-V characteristics

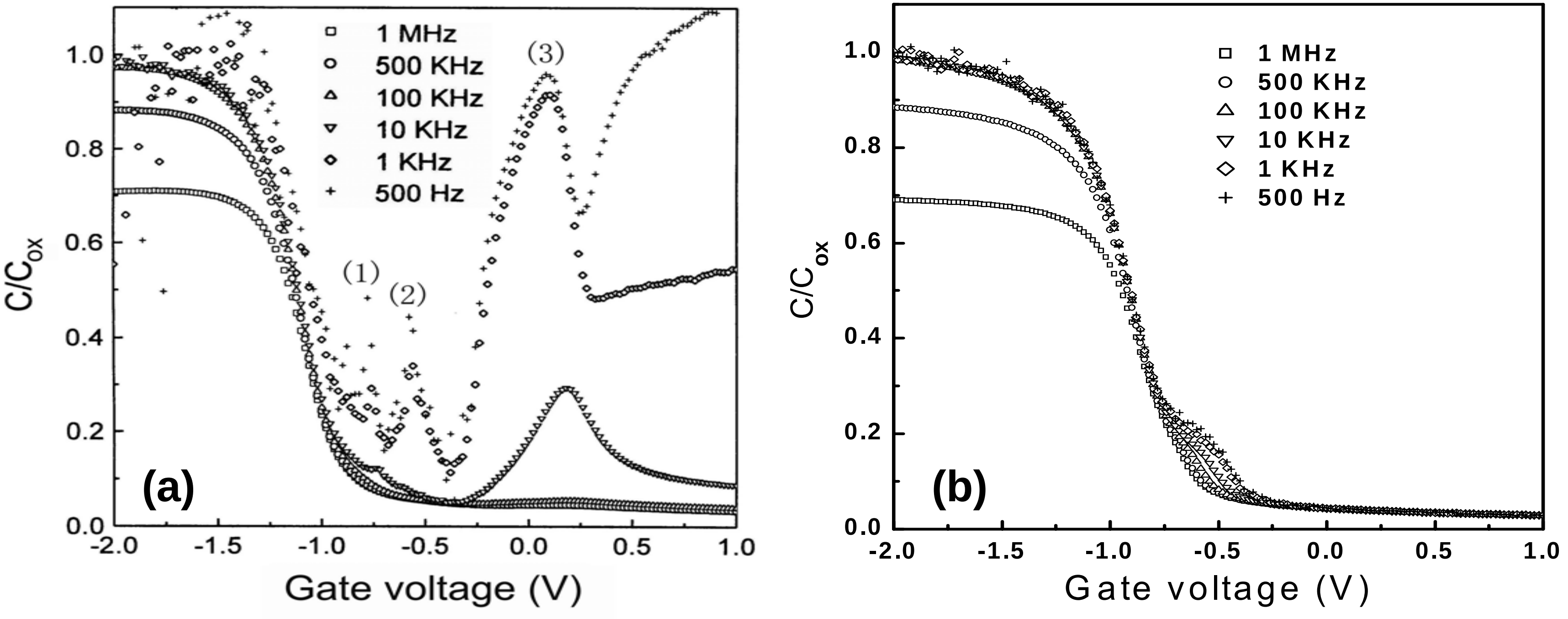

Frequency-dependent C-V characteristics of the samples

(a) with well-defined Si-QDs, in which discrete capacitance peaks are observed;

(b) The reference sample without Si-QDs, in which no peaks are observed.

➢ C-V characteristics

Frequency- dependence of C-V of Samples with different size of nc-Si dots measured at room temperature

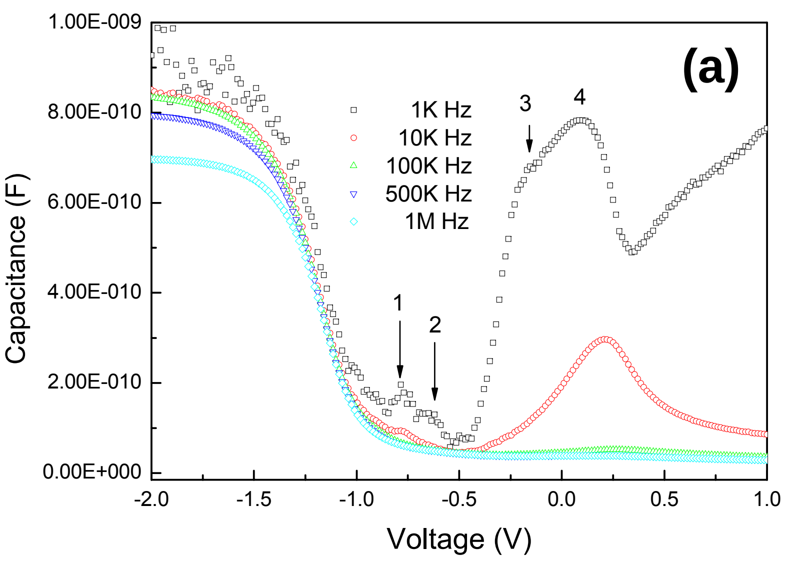

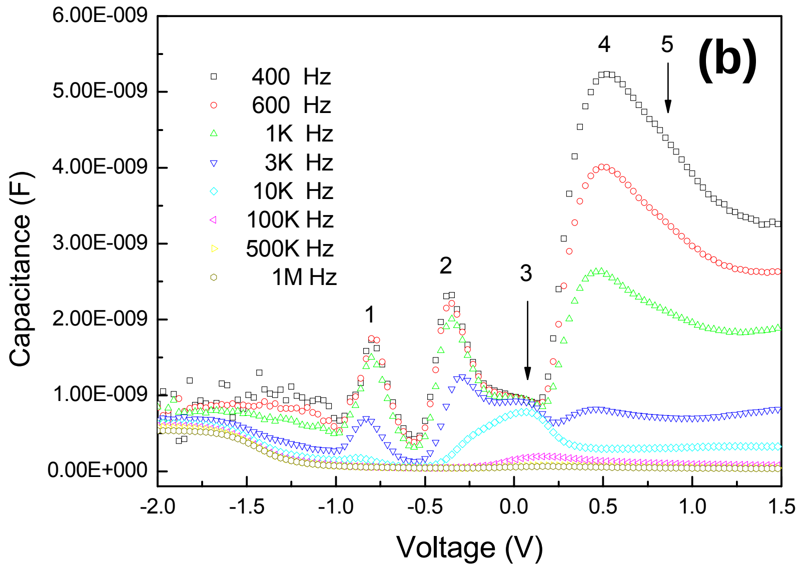

size:	**about 7 nm**	**about 3 nm**
density :	**about 2 x 10^{11} cm^{-2}**	**about 5 x 10^{11} cm^{-2}**

➢ C-V characteristics

Comparisons of theoretical evaluations and experimental results:

Conversion formula between gate voltage difference (ΔV_G) and energy spacing (ΔE):

$$\Delta E = \frac{t_{tun}}{t_{tot}} q \Delta V_G$$

Theoretical evaluations based on Coulomb blockade model

The Coulomb charging energy:

$$E_c = \frac{e^2}{2C_{dot}}$$

where

$$C_{dot} = 4\pi\varepsilon_0\varepsilon_{SiO_2} r$$

➢ C-V characteristics

for radius = 7 nm C_{dot} = *1.49* aF ΔV_G = *0. 17 V*

for radius = 3 nm C_{dot} = *0.64* aF ΔV_G= *0.40 V*

Calculation results:

	7 nm	3 nm
Experiment	50 meV	114 meV
Theoretical	53 meV	125 meV

Experimental results are in accordance with the theoretical evaluations.

Multilevel charge storage in doubly-stacked nc-Si layers

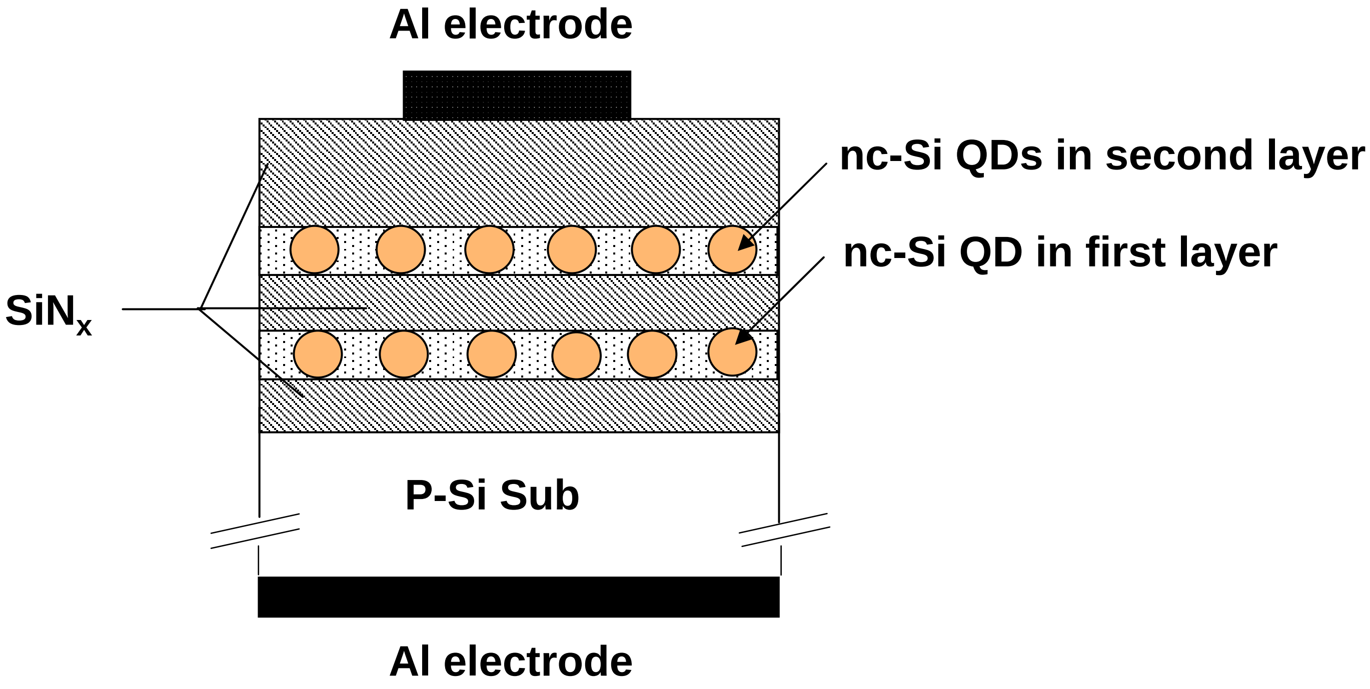

$a\text{-}SiN_x/nc\text{-}Si/a\text{-}SiN_x/nc\text{-}Si/a\text{-}SiN_x$ structure

➢ Charge storage in nc-Si samples

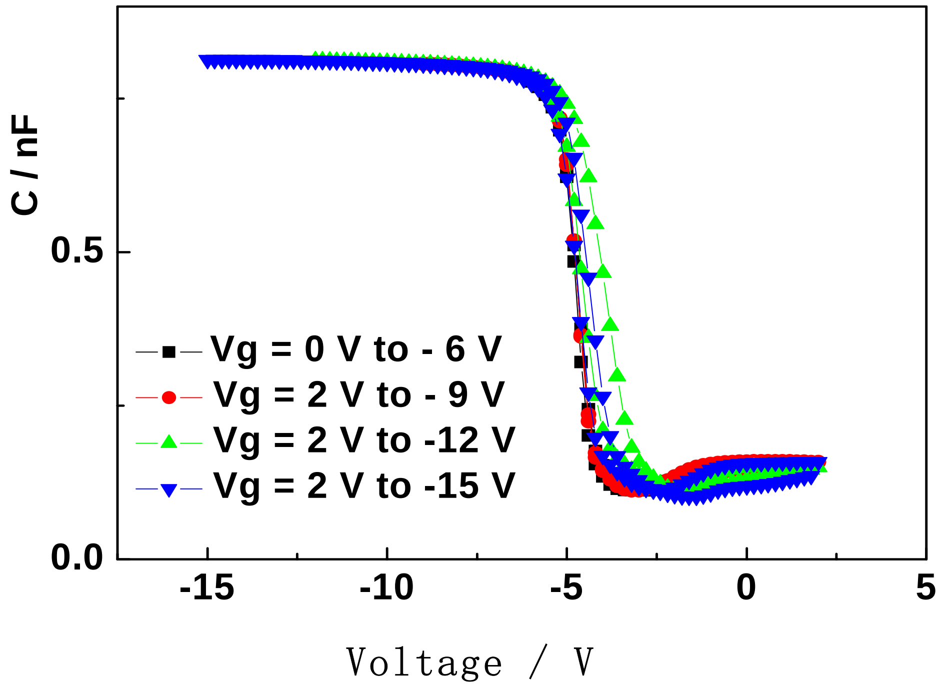

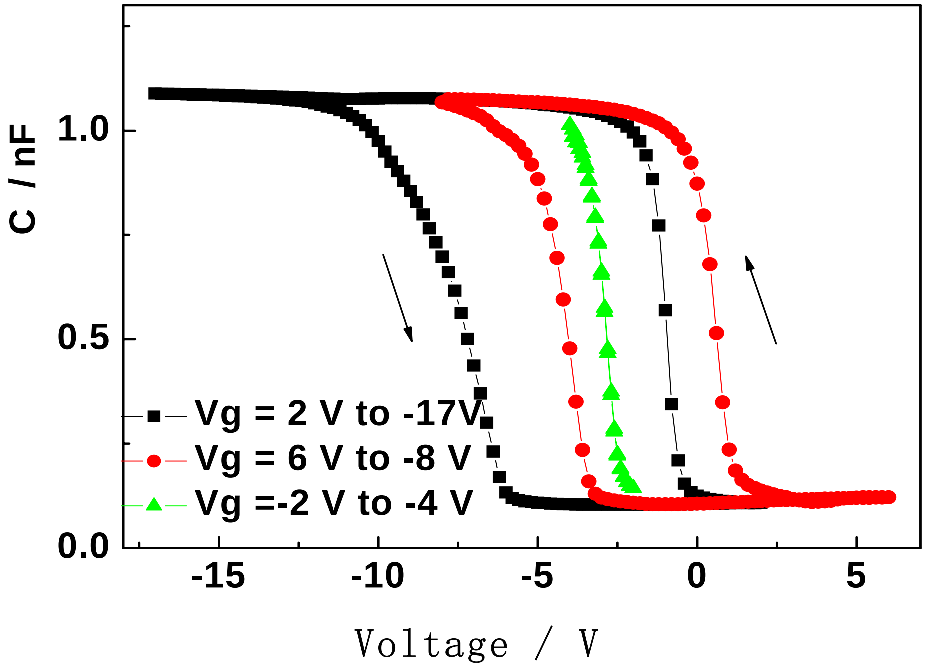

C-V characteristics of
as-deposited samples

(a-SiNx/a-Si/a-SiNx/a-Si/a-SiNx)

C-V characteristics of
samples after annealing

(a-SiNx/nc-Si/a-SiNx/nc-Si/a-SiNx)

➢ Voltage dependence of flat band voltage shift (1)

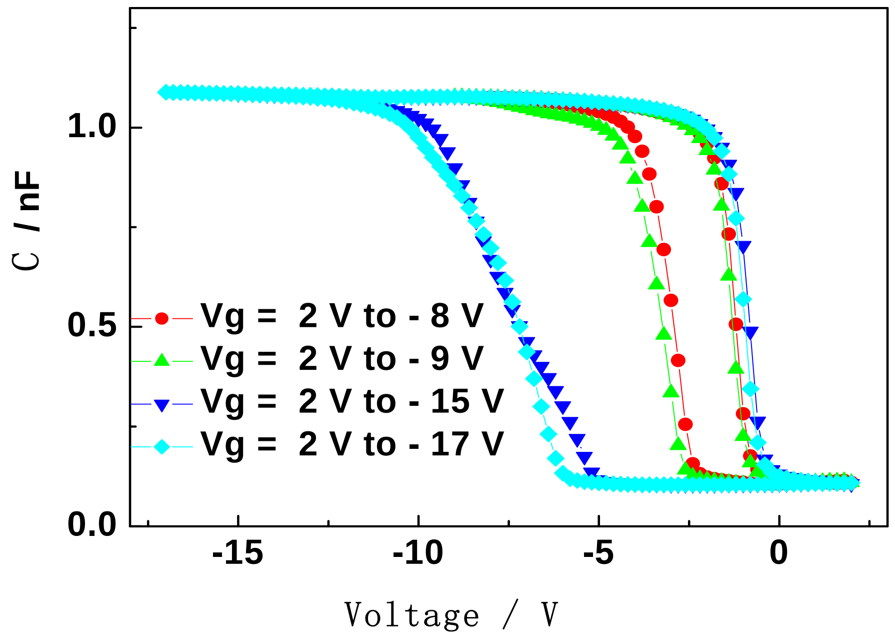

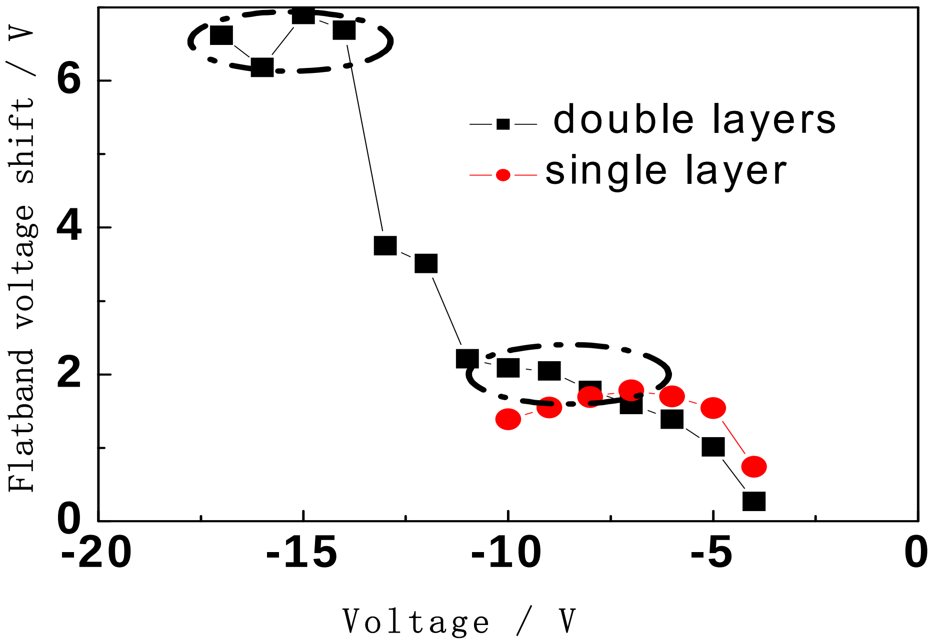

There are two apparent stages observed for the double layers and one stage for the one layer

Holes injected in nc-Si from accumulation region

➢ Voltage dependence of flat band voltage shift (2)

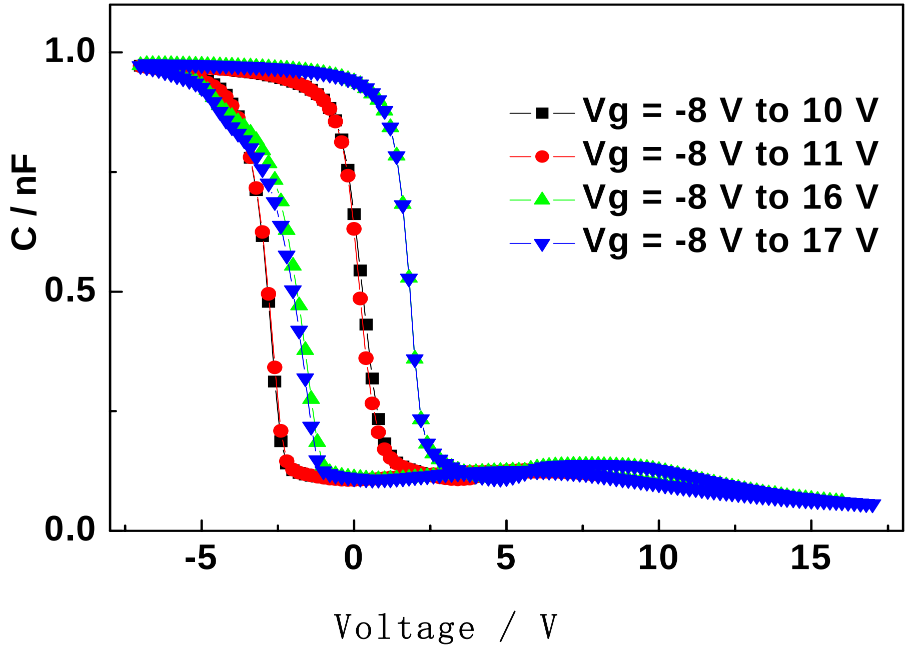

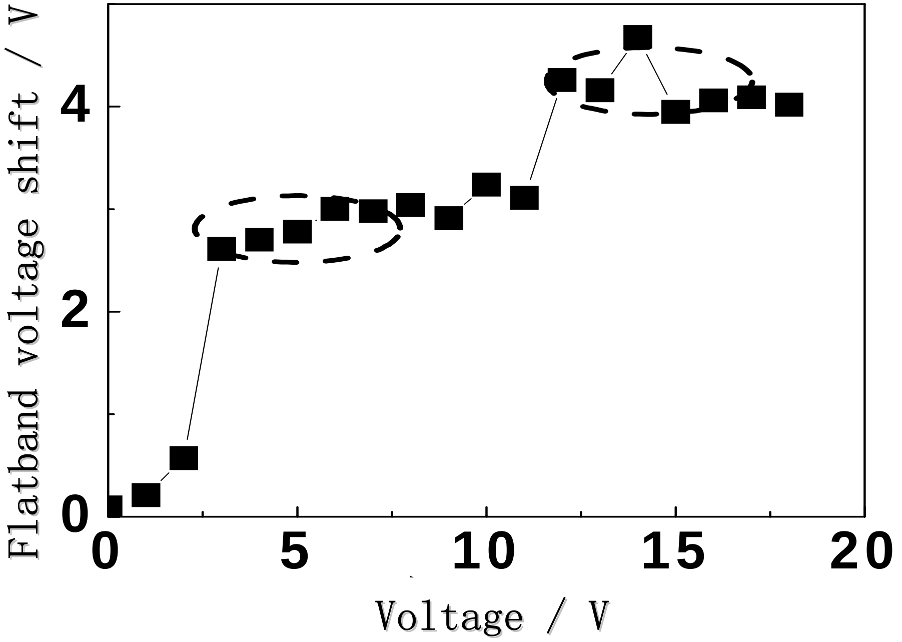

There are two apparent stages observed for the double layers

Electrons injected into nc-Si from inversion region

Multilevel Charge Storage In Doubly-stacked Nc-si Layers

- **Simulation of multilevel charge storage**

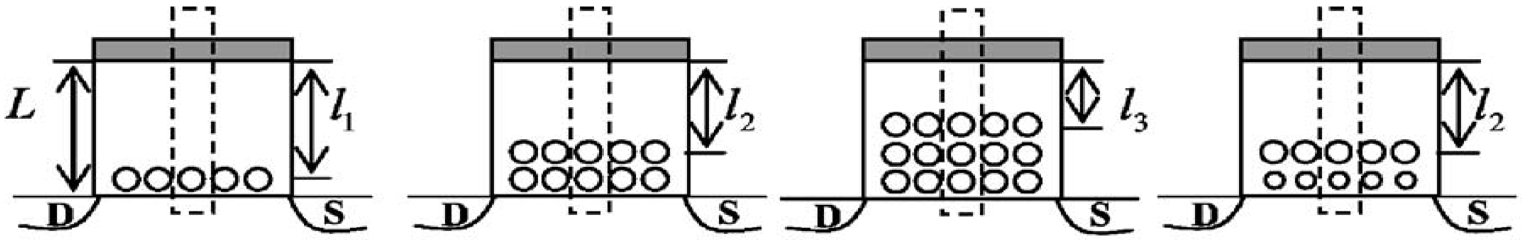

(a) Single layer (b) Double layer (c) Triple layer (d) Asymmetric Double layer

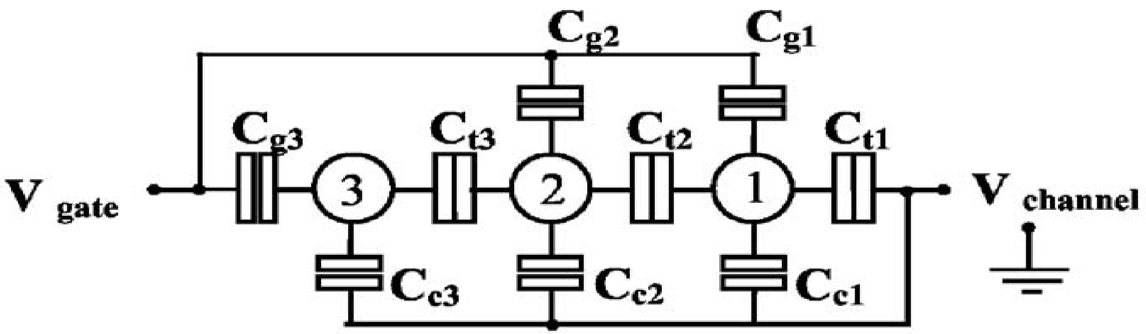

(e) Equivalent circuit for the self-aligned nc-Si unit.

➢ Charging & discharge processes of electrons

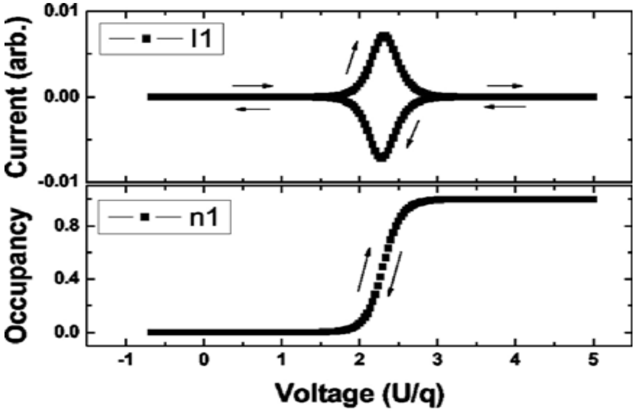

(a)

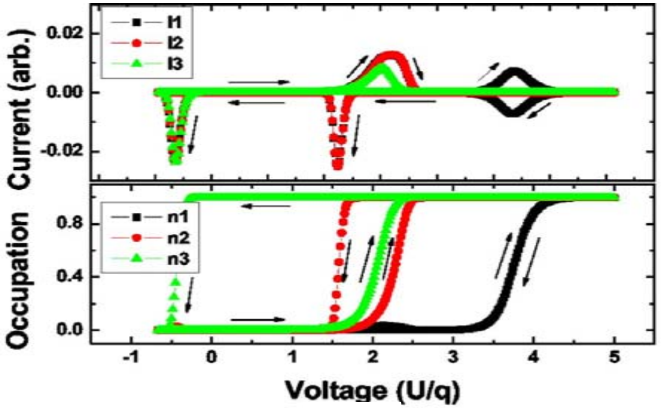

(c)

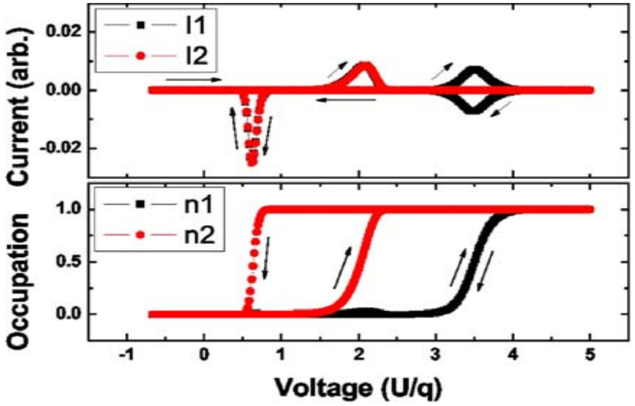

(b)

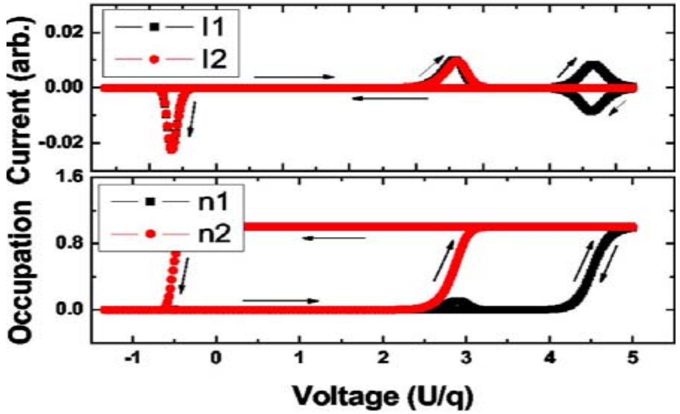

(d)

Resonant Tunneling in Si-rich SiNx / N-rich SiNy Multilayer

➢ Structure

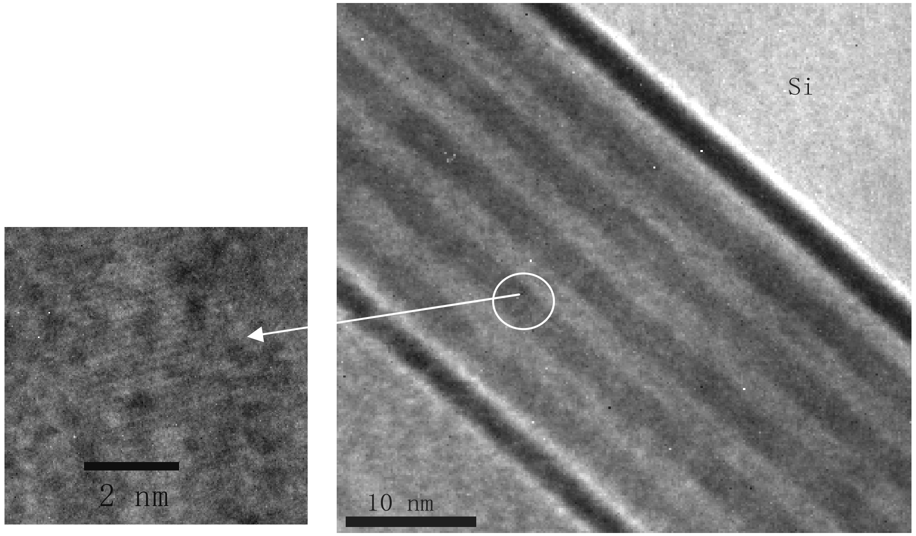

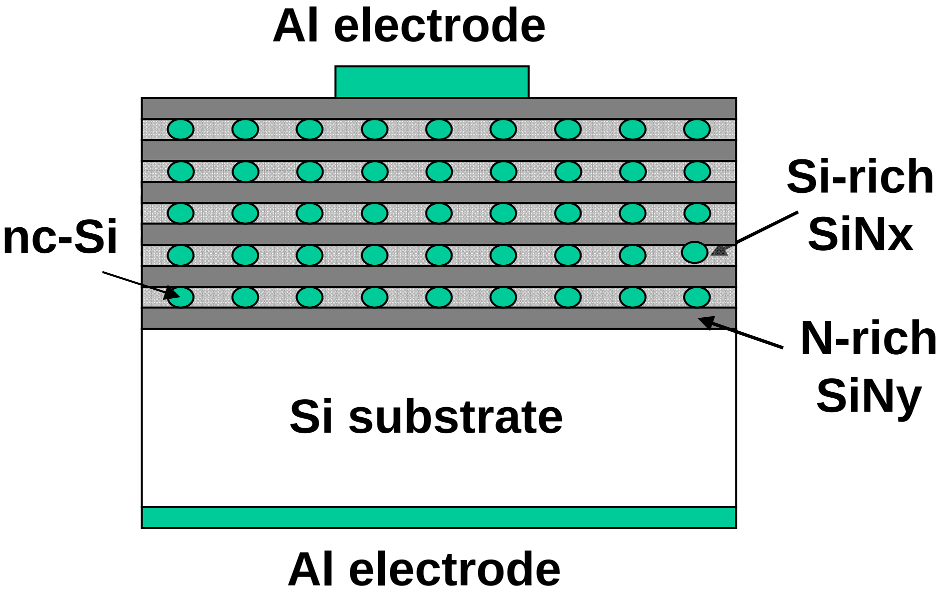

➢ Electrons & Holes resonant tunneling

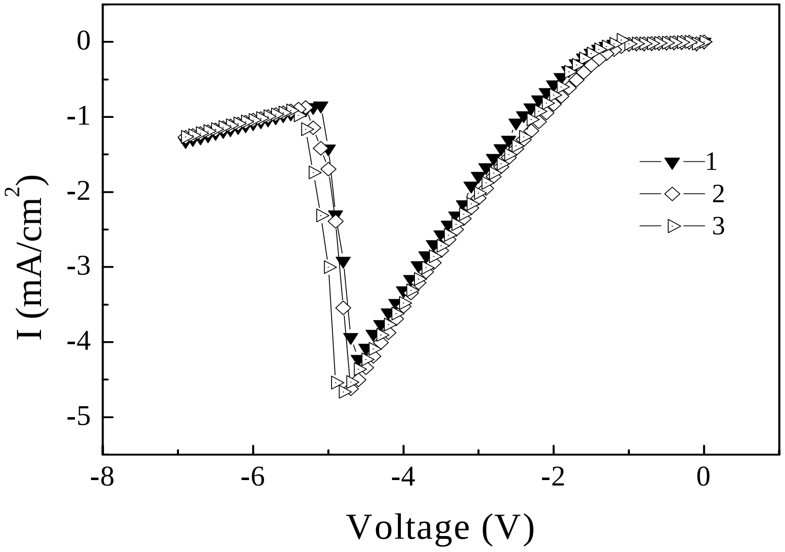

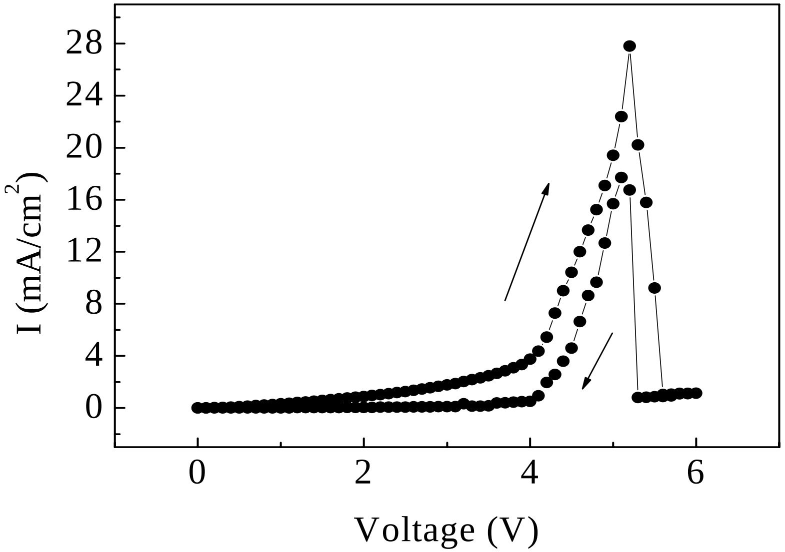

p-type Si Substrate

n-type Si Substrate

Ratio of peak/valley ≈ 5

Ratio of peak/valley ≈ 33

- The collective single-electron Coulomb blockade effects in the uniform 2D nc-Si array have been observed in the I-V and the C-V characteristics.

- The Single-electron memory effects have been studied in a nc-Si floating gate MOSFET. The double-level charge storage in doubly stacked nc-Si in SiNx dielectric has been demonstrated.

提 要

- 引言：研究背景
- 量子点的构筑原理与技术
- 单电子效应及器件应用
- 光子量子点---光子量子化
- 展望

Si基一维光子晶体微腔:

分布Bragg反射器(DBR)设计

$$t = \left| T_{11}^{N} - T_{12}^{N} T_{21}^{N} / T_{22}^{N} \right|^{2}$$

$$r = \left| T_{21}^{N} / T_{22}^{N} \right|^{2}$$

$$P_{l}(d_{l}) = \begin{pmatrix} e^{ik_{l}d_{l}} & 0 \\ 0 & e^{-ik_{l}d_{l}} \end{pmatrix}$$

$$Q_{l,l-1} = \begin{pmatrix} 1/2 + k_{l-1}/2k_{l} & 1/2 - k_{l-1}/2k_{l} \\ 1/2 - k_{l-1}/2k_{l} & 1/2 + k_{l-1}/2k_{l} \end{pmatrix}$$

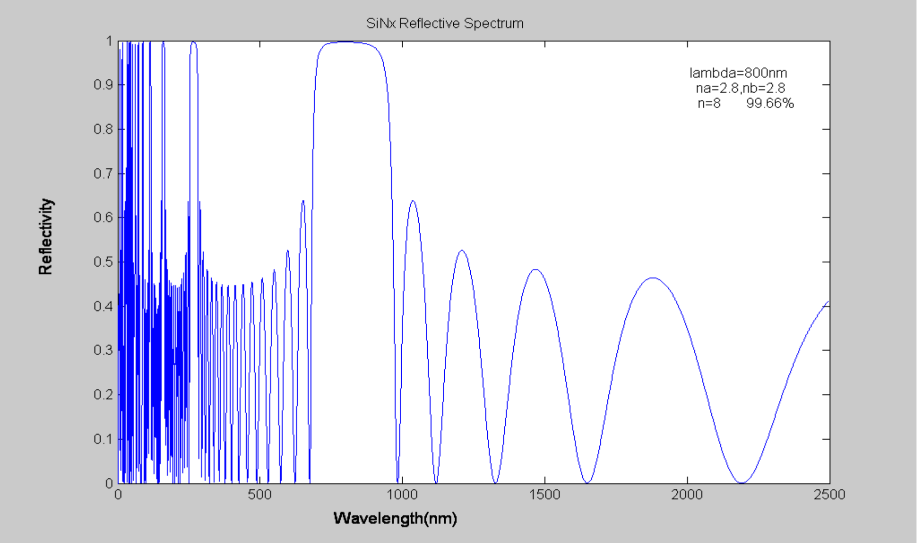

式中 $\boxed{k_{l}}$ 为第 $\boxed{l}$ 子层中的波数。

按照公式，若选用两种材料的**n**分别为**2.8**和**1.86**，周期数为**6**，则计算得到的最高反射率为**98.6％**，最低透射率为**1.4％**。

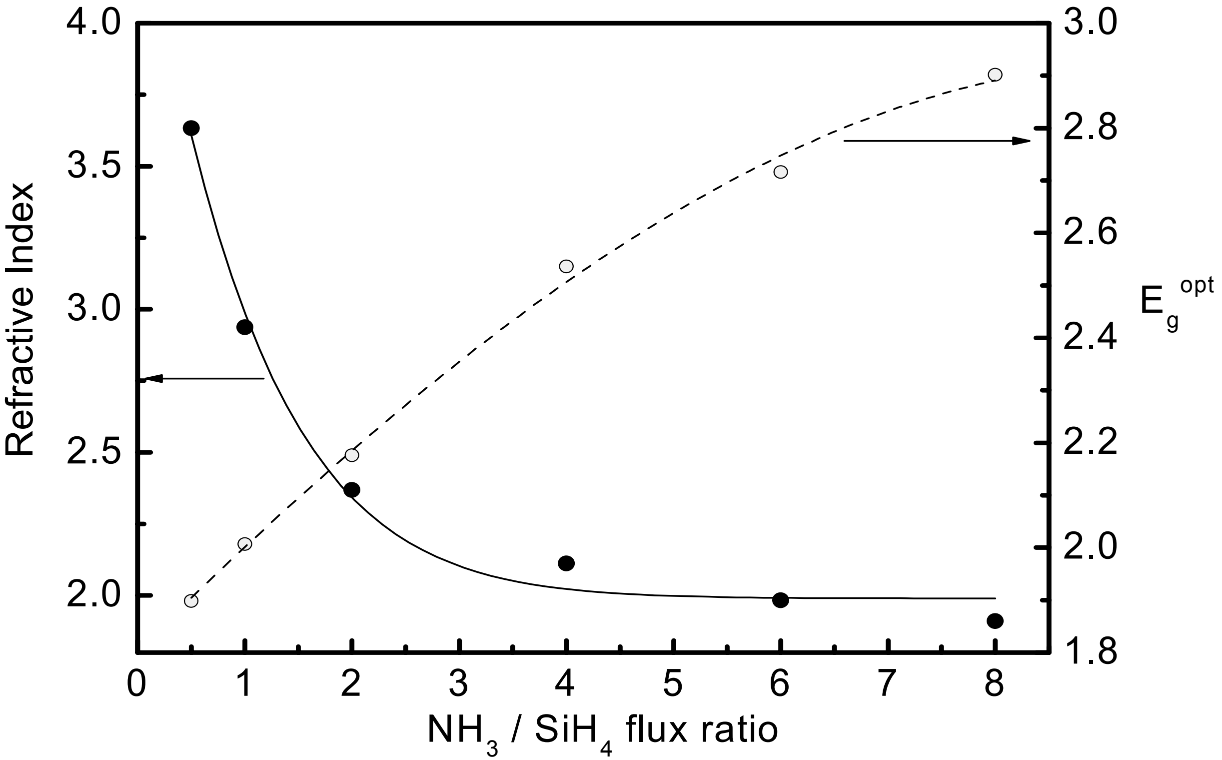

a-SiN_X refractive indices n and optical bandgap E_g^{opt} versus NH_3/SiH_4

a-SiN$_X$光学微腔的示意图与剖面TEM

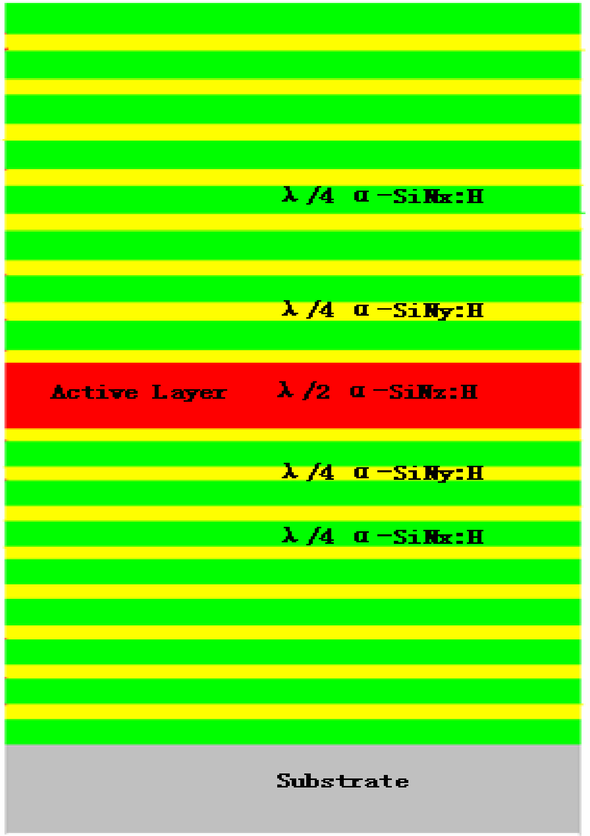

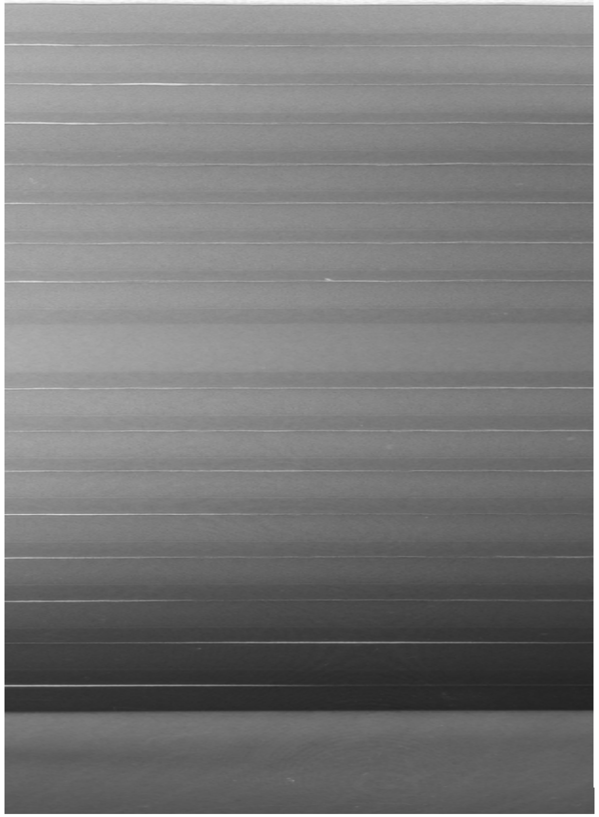

a-SiN$_X$光学微腔的PL谱

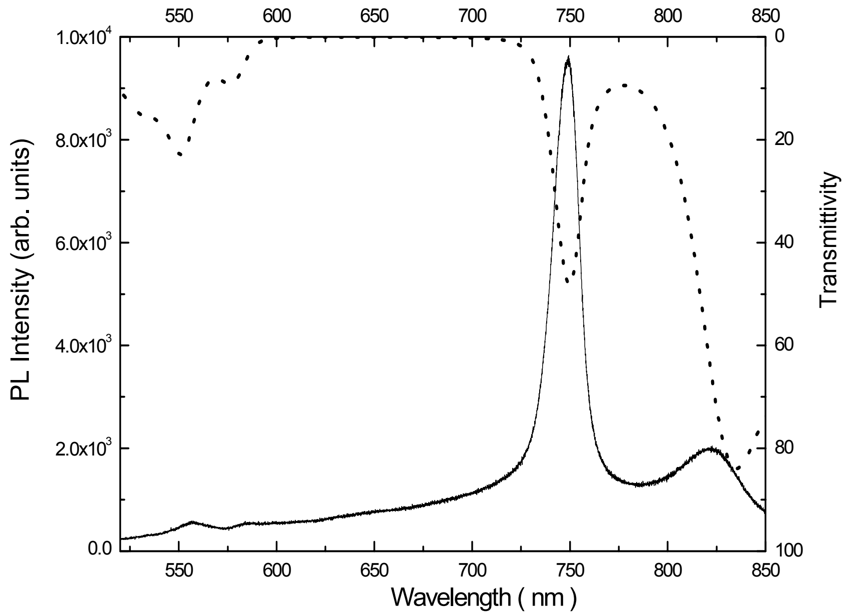

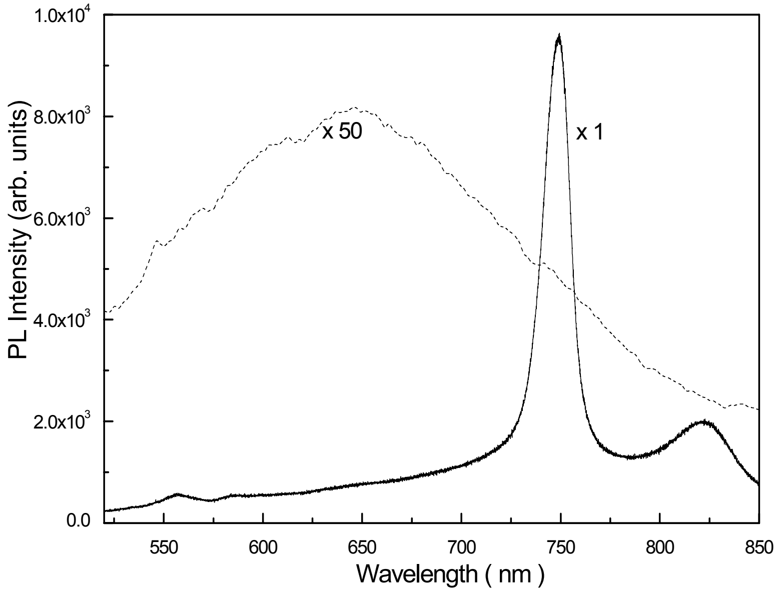

带有λ/2 **a-SiN$_Z$**发光层的一维光子晶体微腔的透射谱和**PL**谱

带微腔的λ/2 **a-SiN$_Z$ PL**谱**(**实线**)**与不带微腔的**a-SiN$_Z$ PL**谱**(**虚线**)**的比较

如何制备Si基3D光学微腔--光子量子点

1. 刻蚀的方法— 形成折射率的不连续

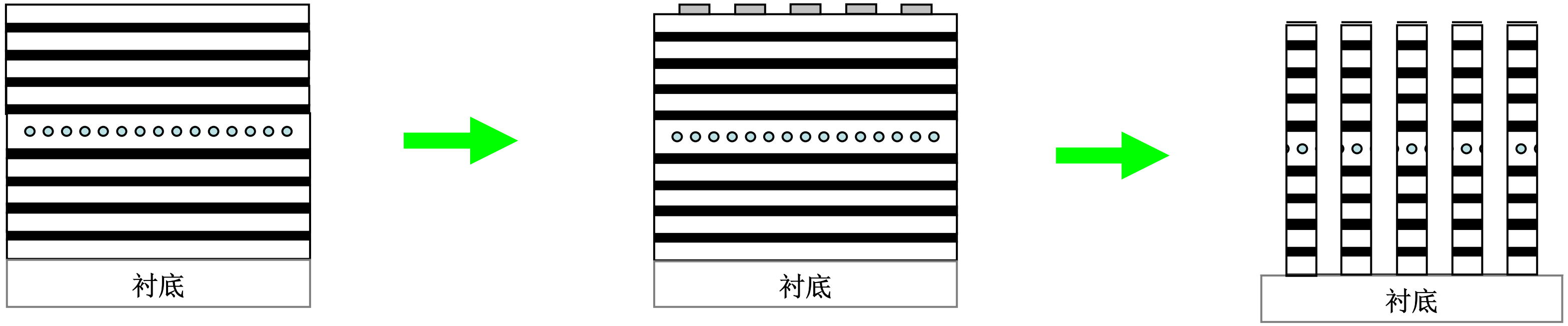

2. 共形生长方法— 构筑全Bragg Reflectors 限制

Si基3D光学微腔--光子量子点

共形生长制备三维微腔光致发光特性

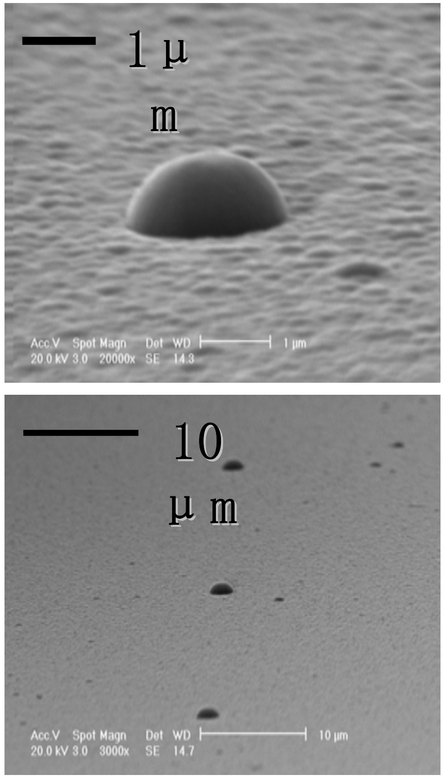

1 μm图形衬底上三维微腔

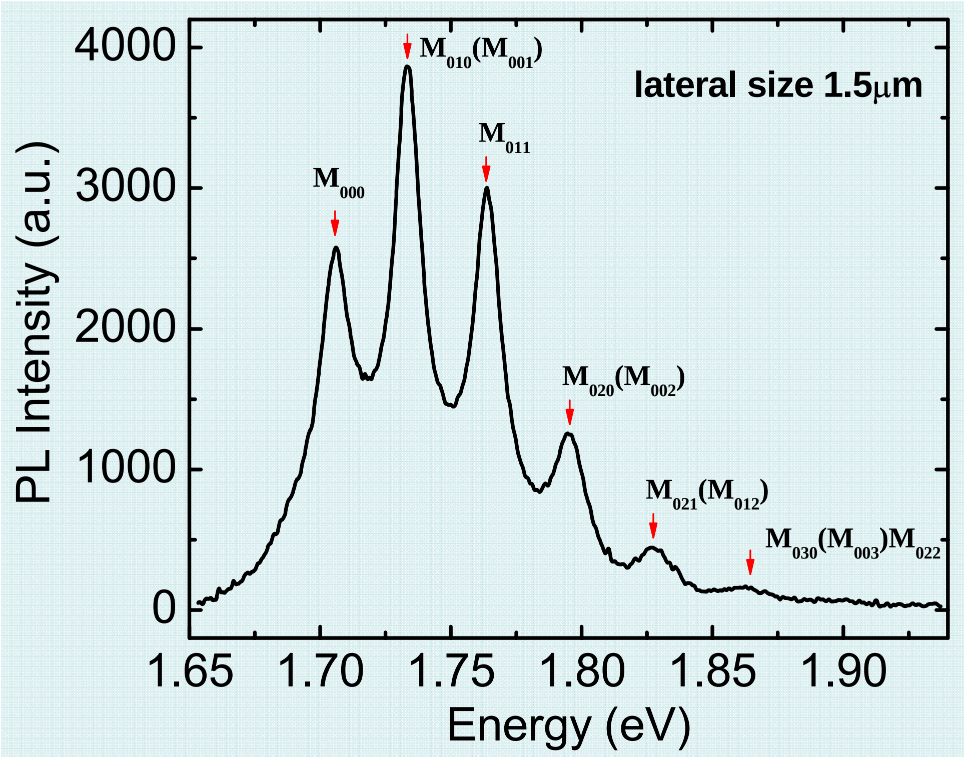

1 μm图形衬底上的微腔PL谱

Si基3D光学微腔--光子量子点

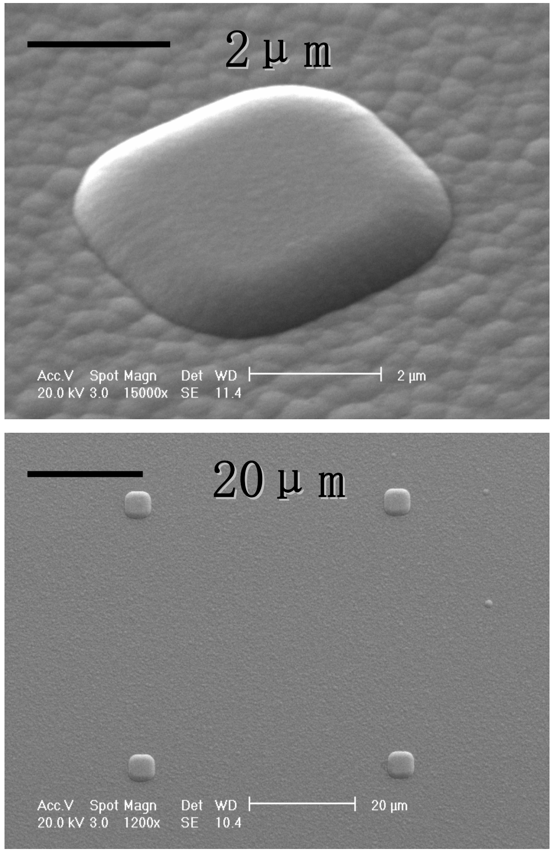

2μm图形衬底上三维微腔

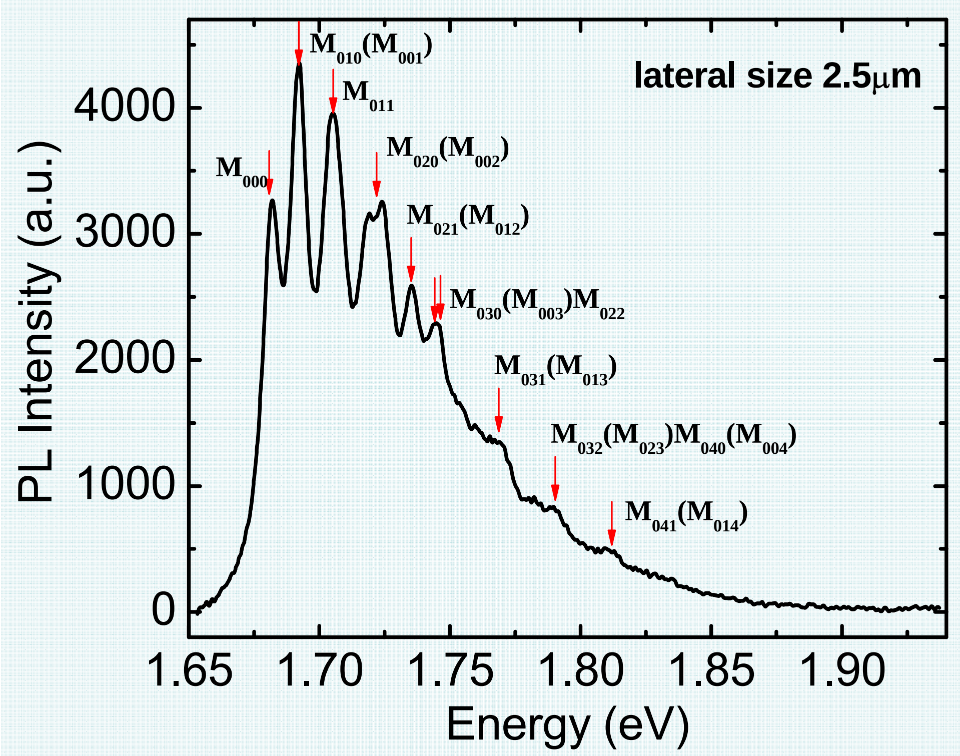

2μm图形衬底上的微腔 **PL** 谱

Si基3D光学微腔--光子量子点

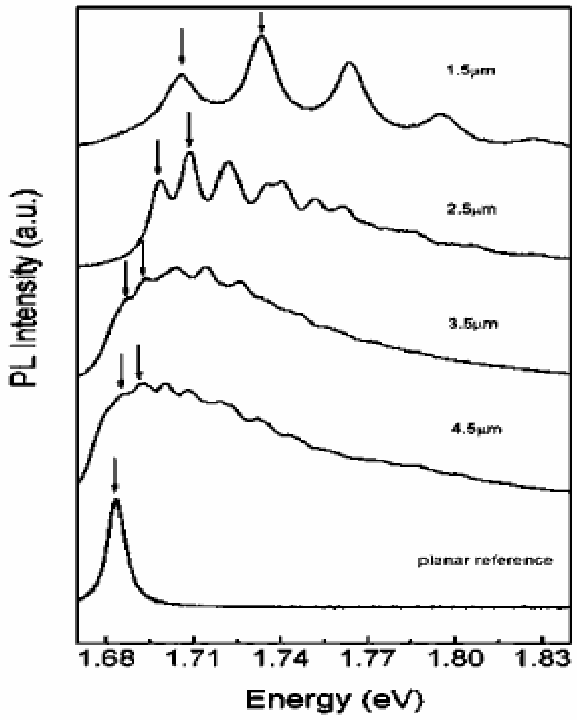

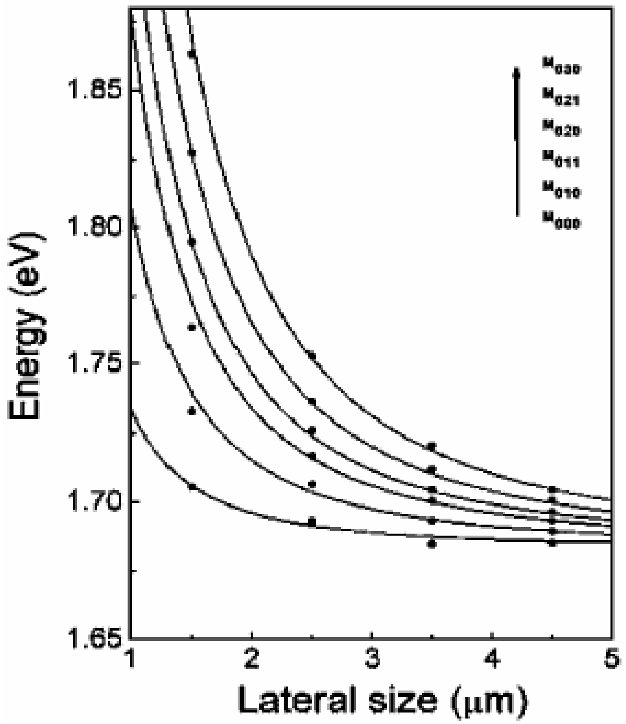

$$E_{ph} = \frac{\hbar c}{n}\sqrt{k_0^2 + k_x^2 + k_y^2},$$

$$k_0 = 2\pi n/\lambda_0, \qquad k_{x,y} = (m_{x,y} + 1)\frac{\pi}{L}.$$

Here $m_{x,y}$= 0,1,2,3,... correspond to the lateral quantum numbers.

Si基3D光学微腔--光子量子点

Lateral size (μm)	M_{000} (eV)	M_{010} / M_{001} (eV)	M_{011} (eV)	M_{020} / M_{002} (eV)	M_{012} / M_{021} (eV)	M_{022} (eV)
1.5	1.705	1.733	1.764	1.795	1.827	1.863
	1.706	1.734	1.773	1.794	1.826	1.868
2.5	1.693	1.706	1.717	1.726	1.737	1.753
	1.691	1.704	1.716	1.724	1.736	1.752
3.5	1.685	1.693	1.701	1.705	1.712	1.721
	1.686	1.694	1.700	1.704	1.710	1.719
4.5	1.685	1.689	1.693	1.697	1.701	1.704
	1.686	1.690	1.693	1.696	1.700	1.705

Table II listed the results of measured energy of the resonant modes for the dots with different lateral sizes compared with calculated values based on 3D confinement model.

光子量子点部分理论模拟结果

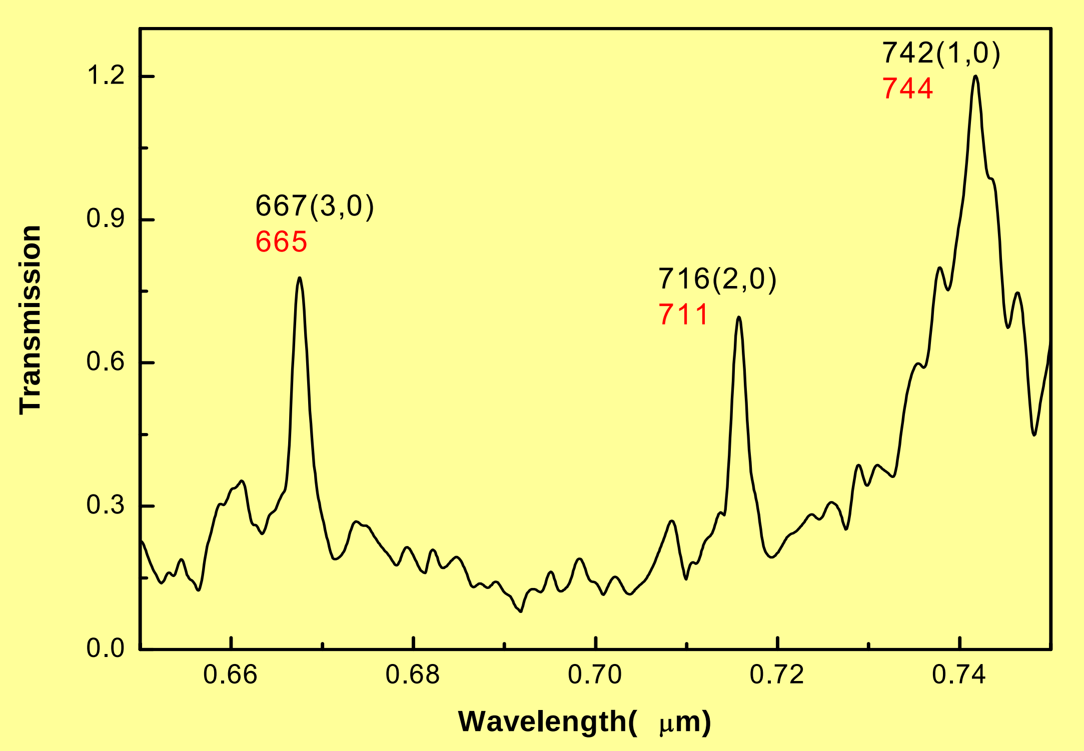

截面为方形光子量子点的透射谱的FDTD数值模拟结果。黑色字体为FDTD模拟的模式位置，红色为理想三维限制模型所得到的模式位置。

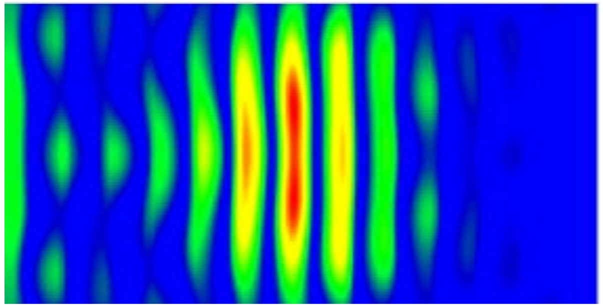

一阶模式光场分布

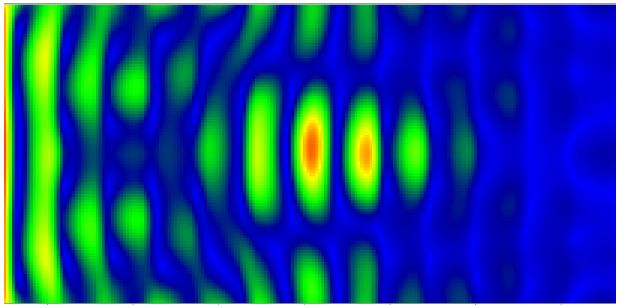

二阶模式光场分布

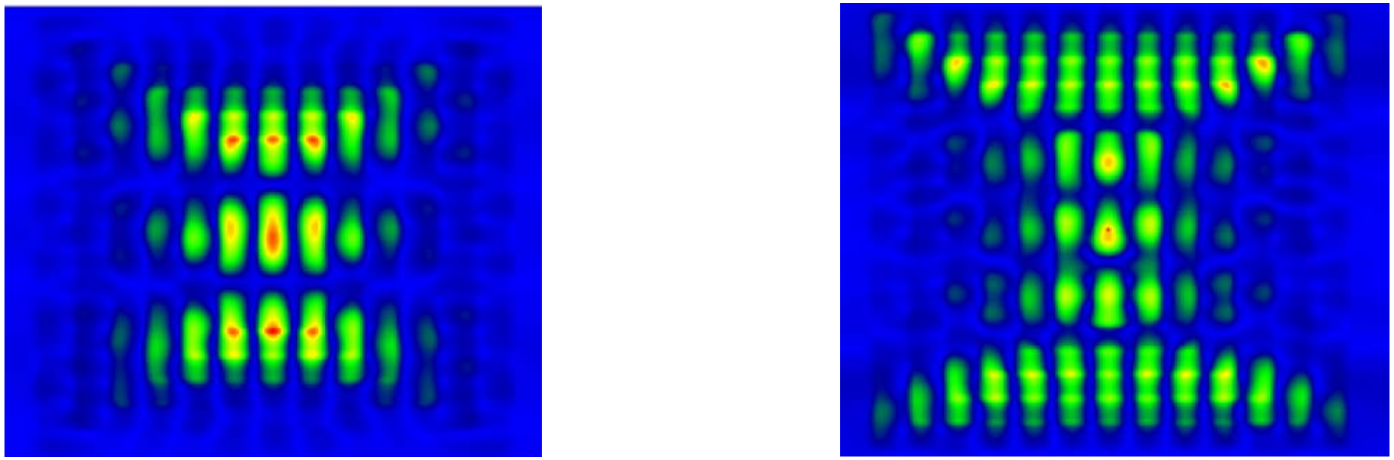

高阶模式光场分布

圆柱形光子量子点低阶和高阶模式光场分布

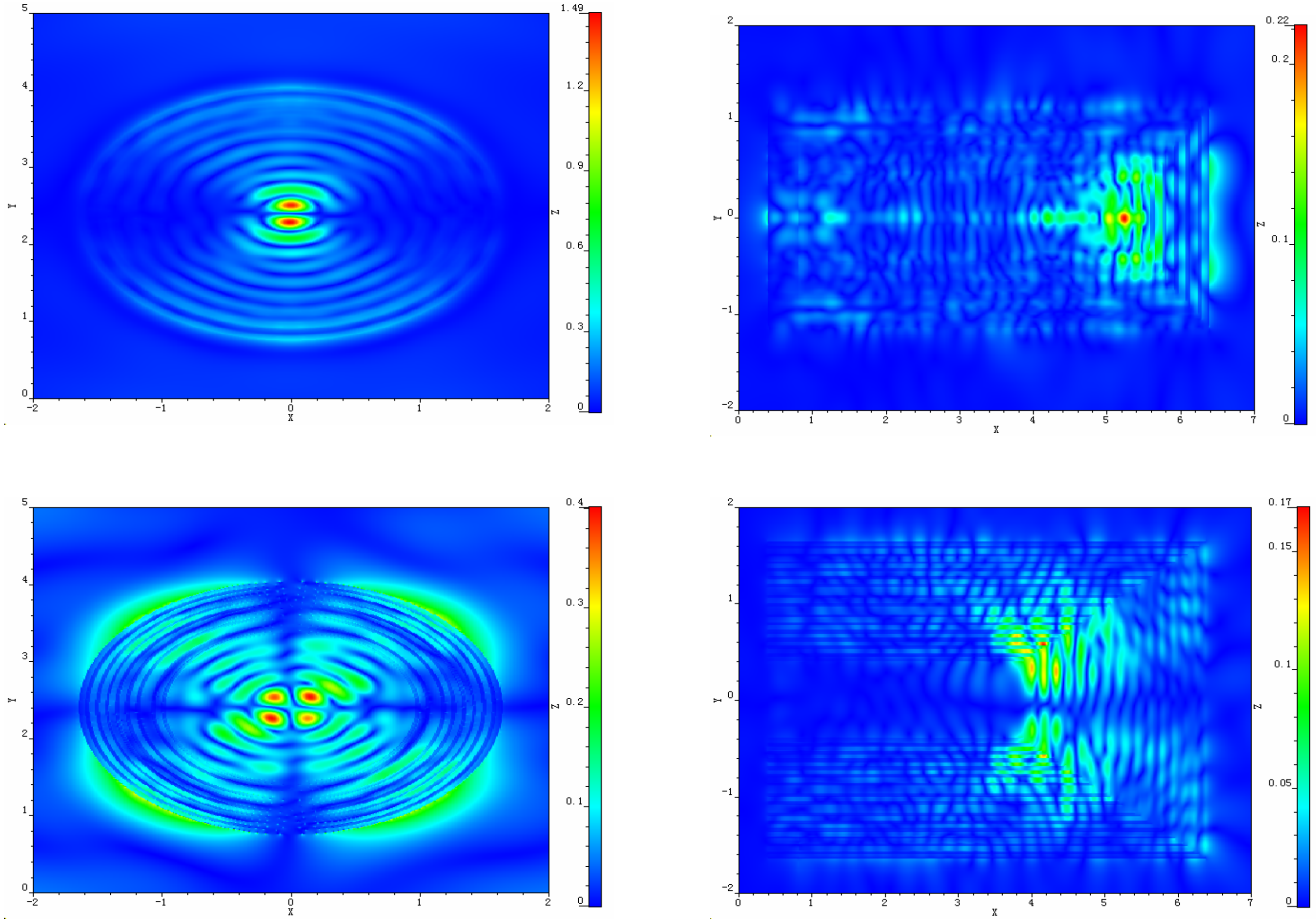

从光子量子点原子到光子量子点分子

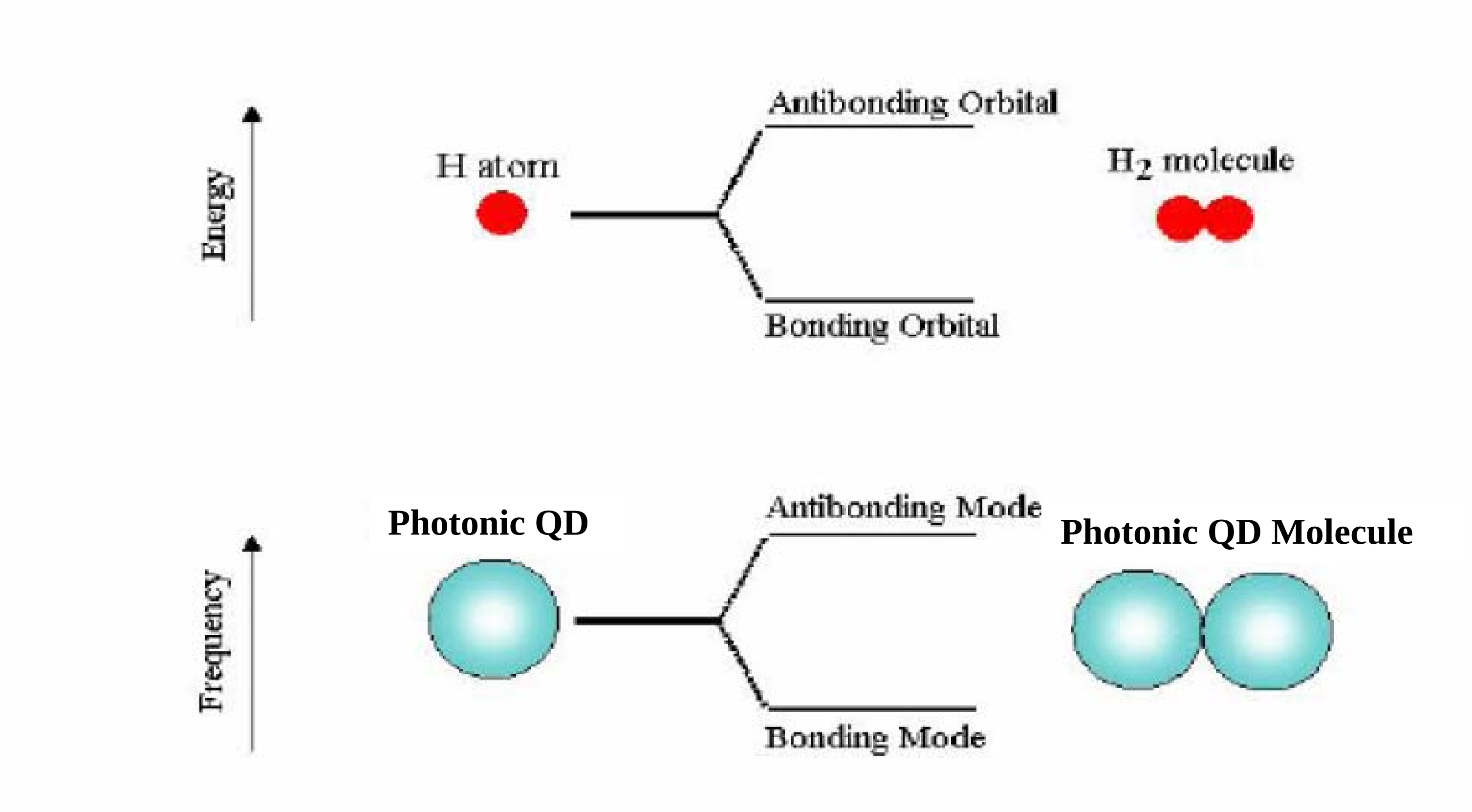

双量子点构成的光子分子与
双原子构成的H_2分子对比示意图

两个光子量子点耦合结构示意图和剖面TEM照片

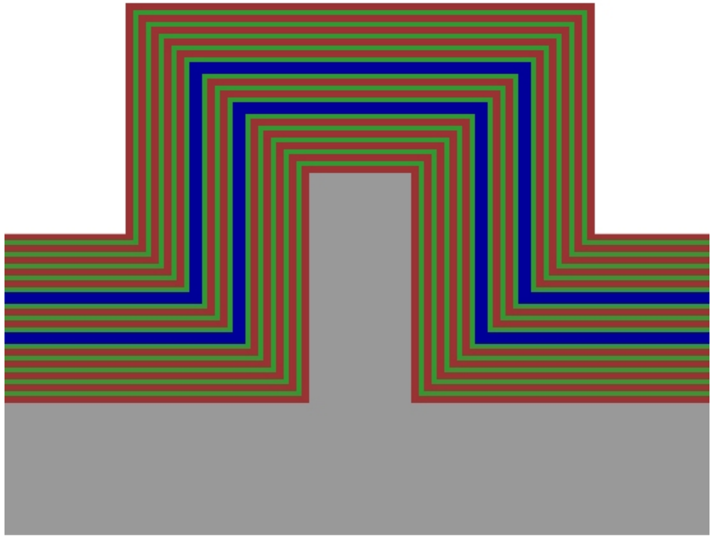

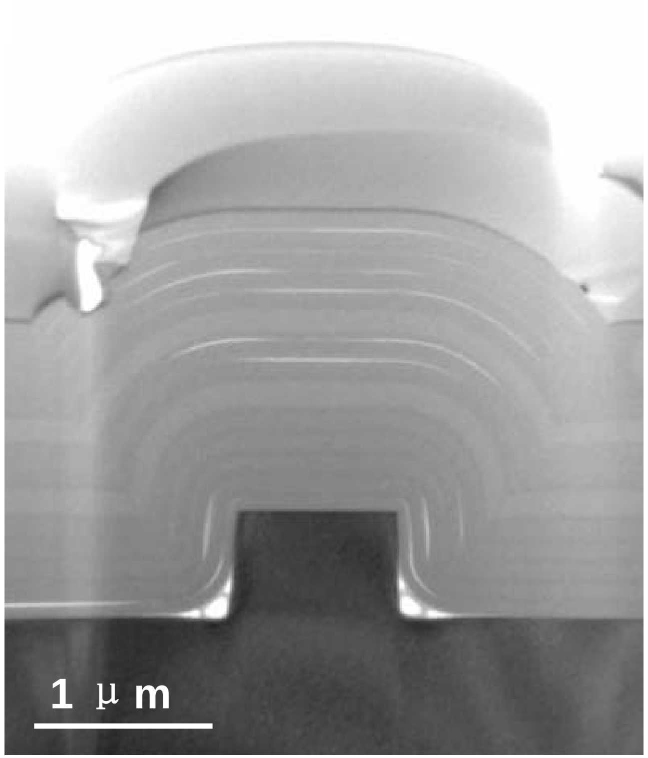

耦合层为2.5个周期的DBR

光子量子点 分子的PL谱

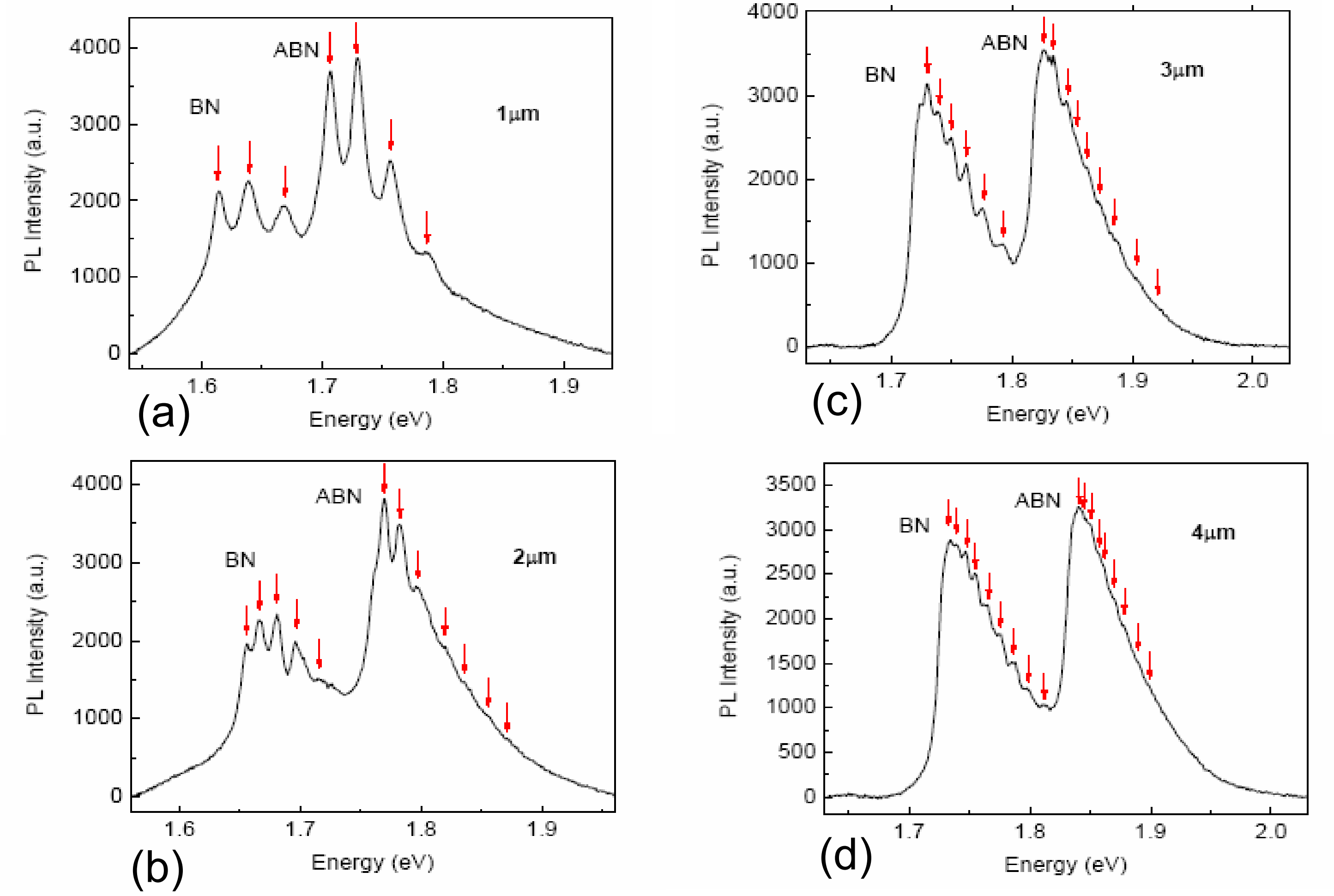

耦合层为2.5个周期DBR的A组光子分子的PL谱

提 要

- 引言：研究背景
- 量子点的构筑原理与技术
- 单电子效应及器件应用
- 光子量子点---光子量子化
- 展望

研究思路的延伸— 人造原子到人造分子

A quantum dot size $L \sim \lambda_F < l_\phi$

λ_F:Fermi wavelength

l_ϕ :phase coherence length

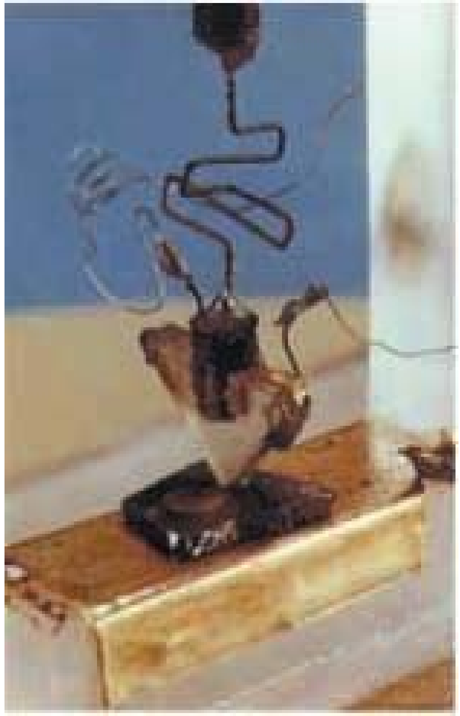

cm → mm → μm → nm

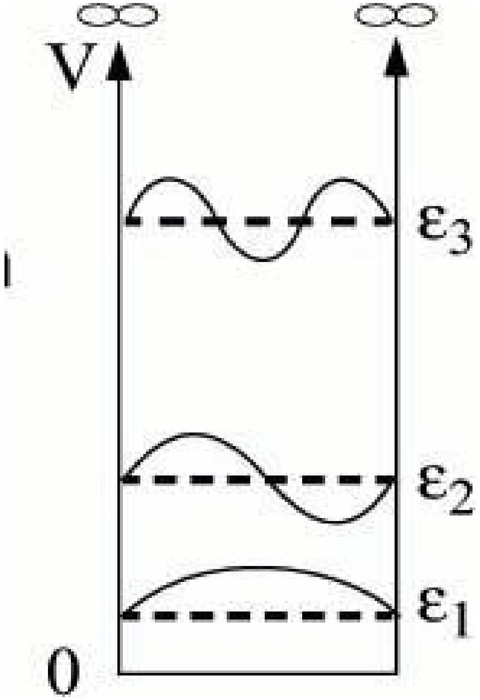

由量子点组成的人造原子、人造分子

artificial atom

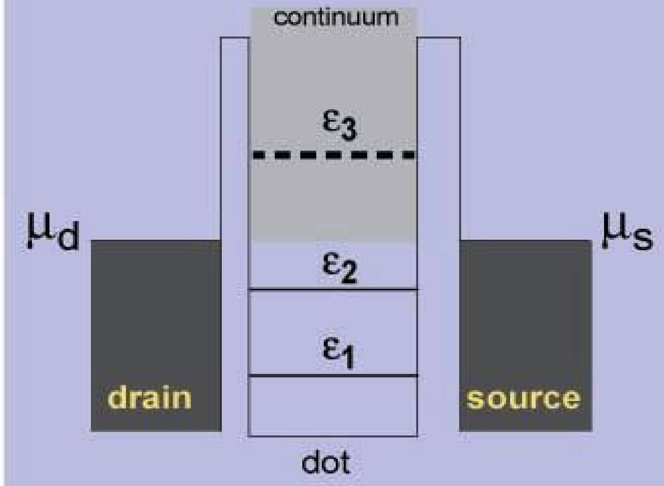

ε_1, ε_2, ε_3, ...

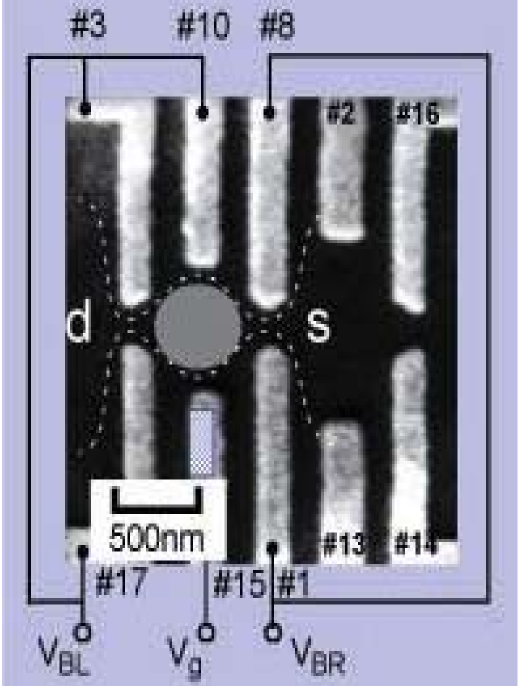

r = 300 nm, N ~ 200

artificial molecule

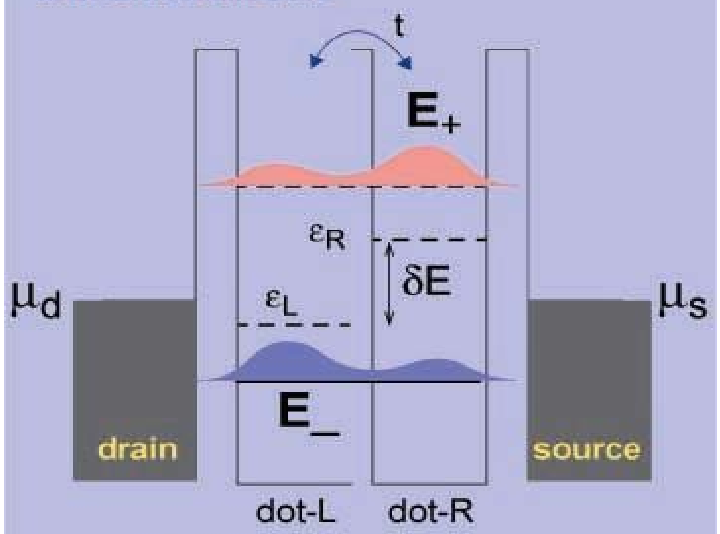

E_+ : anti-bonding state

E_- : bonding state

t : tunnel coupling

$$E_+ - E_- = \sqrt{(\delta E)^2 + 4t^2}$$

人造分子的电子态构成的量子计算比特（**quantum bit**）

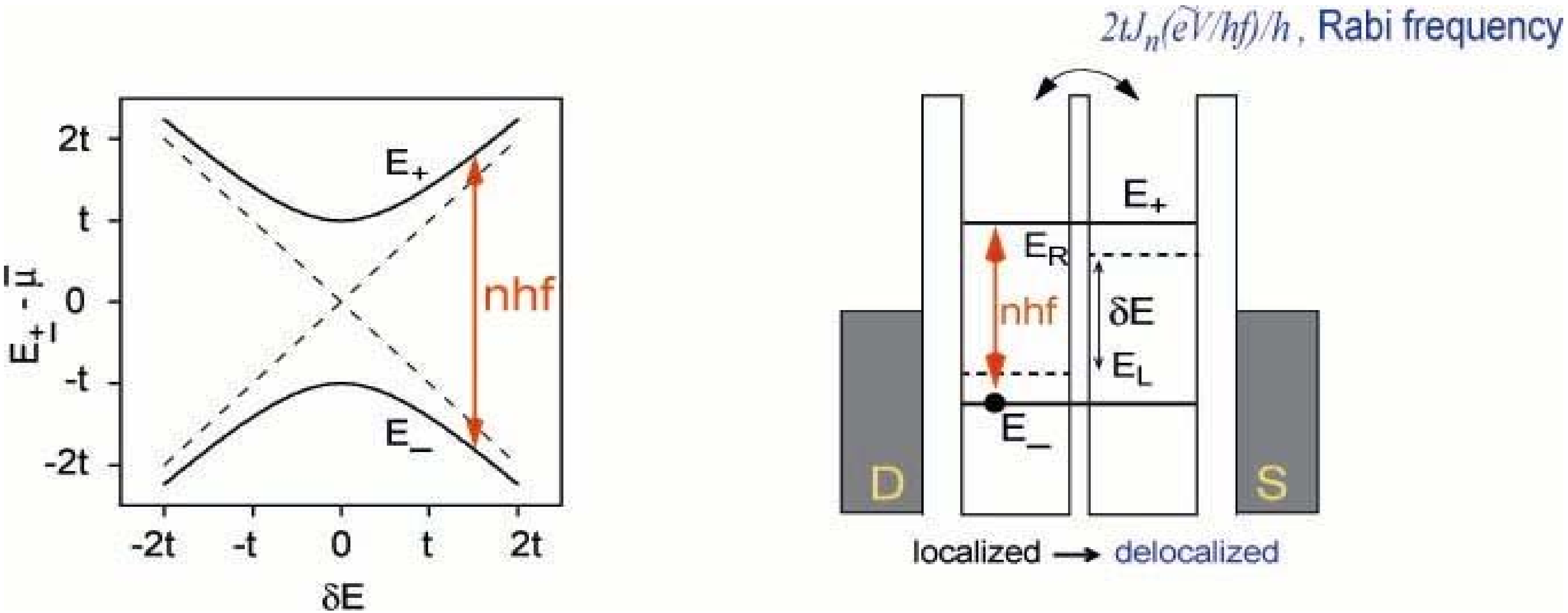

In a artificial molecule, the two electron states can be coupled by external microwave photos when

$$nhf=E_{+}-E_{-}=[(\delta E)^2+4t^2]^{0.5}$$

由两个Si量子点组成的人造分子--- Qbit

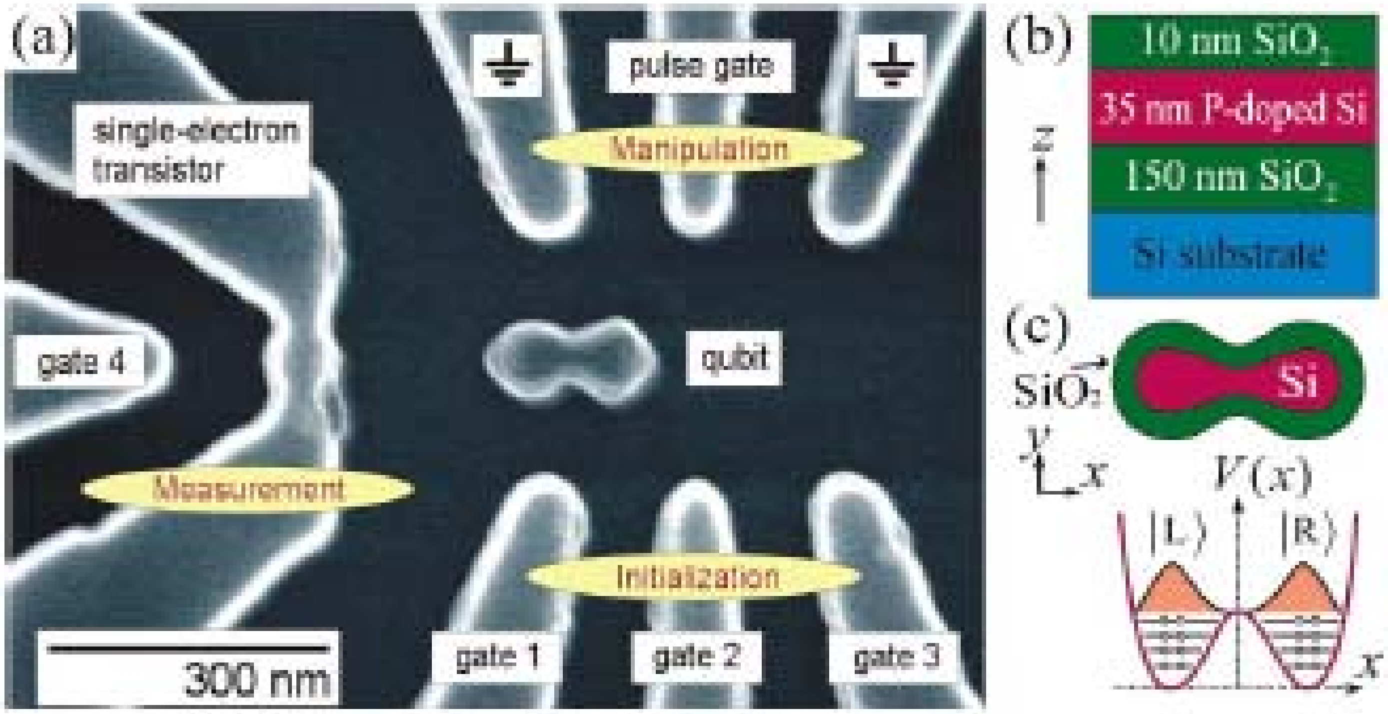

由两个Si量子点组成的人造分子--- Qbit

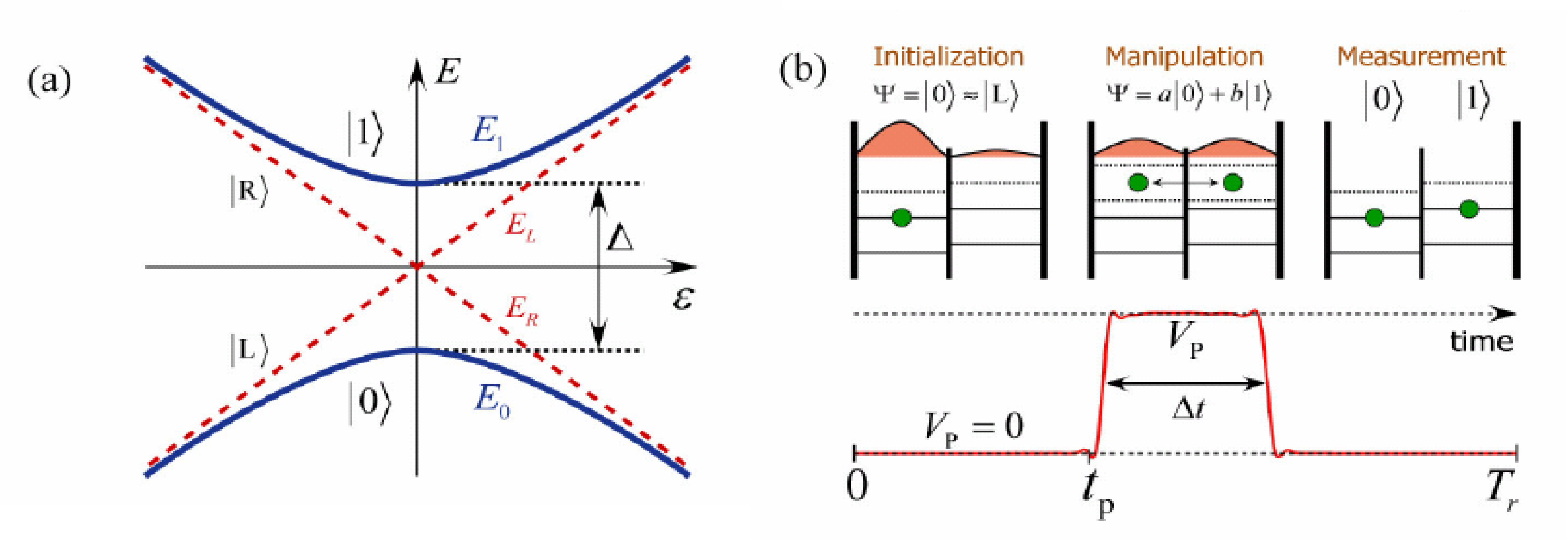

Quantum bit:

$$|t > = a(t)|1> + b(t)|2>$$

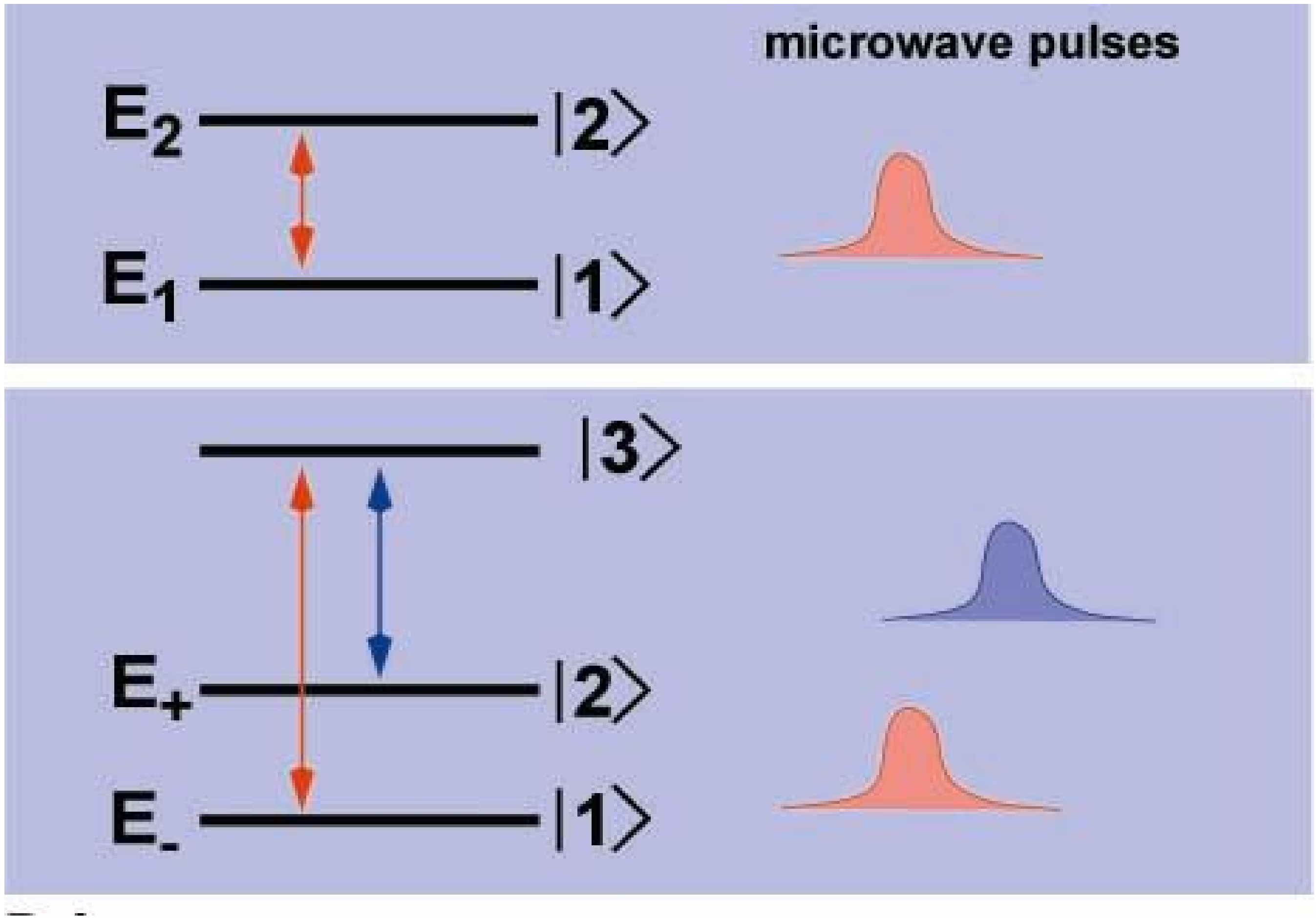

量子点超晶格—人造晶体

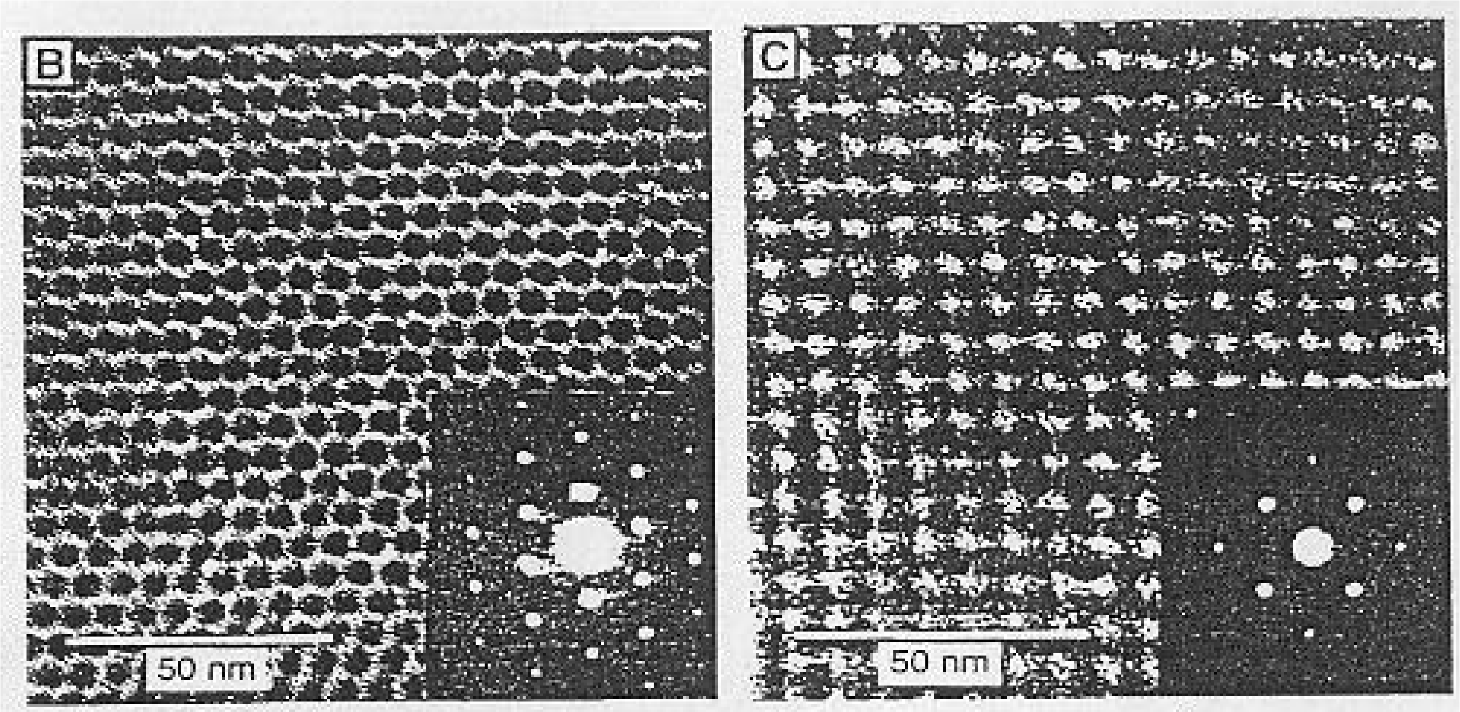

<101>取向 <100>取向

CdSe纳米晶粒构成的三维量子点超晶格,粒径 4.8 nm

小结

- 以量子力学和固体能带理论为基础
- 借助于现代纳米技术
- 我们能够制备出：

人造原子 → 半导体量子点　　单电子晶体管
人造原子 → 光子量子点　　单光子器件

人造分子　　量子点的耦合　　量子计算比特

人造晶体　　3D量子点的有序排列

新的物理现象和器件

谢谢！